ACS NANO

www.acsnano.org

ARTICLE

Delivery, Fate, and Mobility of Silver Nanoparticles in Citrus Trees

Yiming Su, Vanessa E. T. M. Ashworth, Nicholas K. Geitner, Mark R. Wiesner, Nichole Ginnan, Philippe Rolshausen, Caroline Roper, and David Jassby*

Cite This: *ACS Nano* 2020, 14, 2966–2981

Read Online

ACCESS | Metrics & More | Article Recommendations | Supporting Information

ABSTRACT: **Crop disease control is crucial for the sustainable development of agriculture, with recent advances in nanotechnology offering a promising solution to this pressing problem. However, the efficacy of nanoparticle (NP) delivery methods has not been fully explored, and knowledge regarding the fate and mobility of NPs within trees is still largely unknown. In this study, we evaluate the efficiency of NP delivery methods and investigate the mobility and distribution of NPs with different surface coatings (citrate (Ct), polyvinylpyrrolidone (PVP), and gum Arabic (GA)) within Mexican lime citrus trees. In contrast to the limited delivery efficiency reported for foliar and root delivery methods, petiole feeding and trunk injection are able to deliver a large amount of NPs into trees, although petiole feeding takes much longer time than trunk injection (7 days vs 2 h in citrus trees). Once NPs enter plants, steric repulsive interactions between NPs and conducting tube surfaces are predicted to facilitate NP transport throughout the plant. Compared to PVP and Ct, GA is highly effective in inhibiting the aggregation of NPs in synthetic sap and enhancing the mobility of NPs in trees. Over a 7 day experimental period, the majority of the Ag recovered from trees (10 mL, 10 ppm GA-AgNP suspension) remain throughout the trunk (81.0% on average), with a considerable amount in the roots (11.7% on average), some in branches (4.4% on average), and a limited amount in leaves (2.9% on average). Furthermore, NP concentrations during injection and tree incubation time postinjection are found to impact the distribution of Ag in tree. We also present evidence for a transport pathway that allows NPs to move from the xylem to the phloem, which disperses the NPs throughout the plant architecture, including to the roots.**

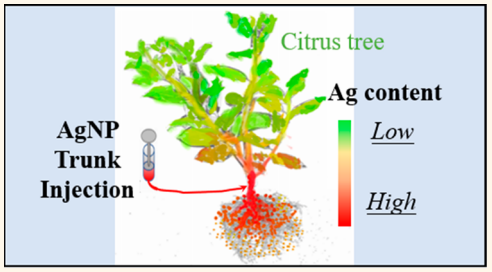

KEYWORDS: *silver nanoparticles, citrus tree, plant disease control, nanoparticle delivery, nanoparticle distribution in tree*

The world demand for fruit and vegetables has been steadily increasing,[1] but production growth has decelerated over the same period.[2] According to Siegel *et al.*,[3] the global supply of fruit and vegetables fell 22% short of demand in 2009, and this shortage will likely worsen. Among the reasons for the slowing production, plant diseases, particularly those caused by bacteria and fungi vectored by insects, are a growing concern. For example, Huanglongbing (HLB), a lethal disease of citrus, is responsible for $4.5 billion in total economic losses in Florida over a period between 2006 and 2011.[4] HLB is caused by the bacterium *Candidatus Liberibacter asiaticus* (CLas), which is spread by a psyllid and is currently incurable. The pathogen resides primarily in a plant's vascular system (*i.e.*, xylem and/or phloem), where it is hard to eliminate but can readily move throughout the entire plant. It remains challenging to characterize and culture these pathogens and manipulate them genetically.[5] To date, progress has been reported on the control of this type of pathogen *via* plant resistance genes,[6] antibiotics,[7] or introduction of plant growth-promoting bacteria.[8] However, the need for effective methods to control these diseases remains acute. Recent developments in nanotechnology offer a promising avenue toward a curative solution to these diseases.[9,10] Some nanoparticles (NPs) possess excellent antimicrobial properties: copper NPs and zinc NPs are being evaluated for efficacy against CLas or other bacterial pathogens in citrus,[11−13] and silver NPs (AgNPs) have also been evaluated for direct inhibition of plant pathogens.[14,15] In addition, NPs can effectively move within plants (such as tomato, cucumber, wheat), utilizing the plant's vascular system, where they can interact with invading pathogens.[16,17] Nevertheless, several critical issues must be resolved before practical agricultural applications can be made possible.

Received: September 30, 2019
Accepted: March 6, 2020
Published: March 6, 2020

https://dx.doi.org/10.1021/acsnano.9b07733
ACS Nano 2020, 14, 2966–2981

One of the critical questions is how to efficiently introduce NPs into plants (delivery efficacy: the amount of NP entering the plant divided by the total mass of dosed NPs). Foliar application (including NP suspension spray/infiltration,[18] nanoaerosol exposure,[19] vacuum infiltration,[20] and pressurized bath infusion[21]) and root application of NP suspensions (*i.e.*, soil drenching)[22,23] are the most widely reported methods. While foliar spray can deliver NPs to chloroplasts of citrus leaves[24] or in the mesophyll of tobacco leaves,[25] NPs delivered by this technique can be easily washed away by water (over 70% of total NPs dosed on leaves).[26] In addition, the leaf cuticle/epidermis prevents the entry of most NPs, with approximately 80% of NPs penetrating leaves remaining in the first 200 nm beneath the leaf cuticle after 7 days of exposure.[27] In terms of root application, while most NPs remained in culturing media, the epidermis and the Casparian strip (in fully formed root) block the penetration of NPs.[28] Thus, it is very likely that delivery efficacies of foliar and root application are low, although the efficiency of the foliar application appears to be higher than that of the root application.[20,21] To the best of our knowledge, very little effort has been placed on systematically investigating and comparing the efficacy of these methods for NP delivery. Another delivery method, using branch/petiole feeding and trunk injecting, has not received much attention. In a recent report, a feeding/injecting method was used to efficiently deliver plant defense activators, antibiotics, and plasmid DNA.[29−31]

In addition to the delivery method chosen, the mobility of NPs is impacted by a plant's internal environment and the way by which water and solutes, including a high concentration of inorganic/organics and NPs/antimicrobials, move within its vascular tissues, the xylem (upward transport) and the phloem (downward transport).[17,32−34] Both xylem and phloem consist of tube-shaped conduits (vessels in xylem and sieve tubes in phloem) for axial transport. The tube shape is achieved by cells arranged end-to-end whose end walls are perforated to facilitate transport. On their lateral walls, adjacent vessels are connected by pits that are much smaller than perforation plates. Pits straddle the cell walls of both vessels and retain a central membrane, known as the intervessel pit membrane.[35] Individual vessels have a finite length, and continuity of water movement beyond the first vessel is ensured by overlap with an adjacent vessel. Thus, these vessel relays rely on pit connections, including their intervessel pit membranes, through which solutes must pass to enter a new vessel.[36] Once NPs enter a plant, it remains largely unknown how the complex internal environment of the plant (*e.g.*, sap composition,[34,37] sap flow rate,[38,39] and pore sizes of intervessel pit membranes, vessel perforation plates, and sieve plates[37−39]) impact the fate and transport of NPs. Based on previous reports, the high ionic strength of sap can lead to NP aggregation, while the existence of abundant organic molecules may reduce aggregation through steric stabilization.[40−42] Specific ionic species (*e.g.*, chloride,[43] phosphate[44]) or organic macromolecules (*e.g.*, humic acid[45] and extracellular polymeric substances[46,47]) could impact the dissolution rates of NPs, and sap flow rates and pore sizes of a plant's xylem pit membranes or phloem sieve plate pores can impact the deposition and detachment of NPs.[48] Thus, the behavior of NPs in sap needs to be evaluated to better understand the transport of NPs and their distribution in plant tissues. Importantly, the majority of studies exploring the use of NPs in agriculture focus on small annual plants that are easy (and fast) to grow, such as tomatoes, cucumbers, wheat, and watermelon.[18,19,49,50] Few, if any, studies have looked at the fate and transport of NPs in large, woody perennial plants, such as trees. Considering the high value of perennial tree and vine crops, there is a strong economic incentive to develop curative methods specifically tailored to trees, which may justify the cost of NPs.

NP properties, such as their size and surface coating, also impact the behavior of NPs in plants.[51,52] Based on previous studies, small sizes are preferable for epidermis penetration.[52,53] For instance, only NPs smaller than 5.4 nm applied to a citrus leaf entered the phloem;[54] only PVP-coated gold NPs smaller than 10 nm crossed the cuticle layer of a wheat leaf after 2 weeks (PVP, polyvinylpyrrolidone).[49] In addition to size, it appears that surface coating can impact the transport of NPs within a plant. Surface coatings change the surface hydrophobicity and surface charge as well as provide steric stabilization.[49,55−59] It has been reported that, in foliar applications, while a PVP coating enhanced NP uptake by a wheat leaf compared to a citrate coating (same metallic size for both coated NPs), the citrate coating allowed more efficient transport of NPs to the plant's vasculature (after penetrating epidermis) due to its hydrophilic character.[49] However, in root applications, a PVP coating facilitated the transport of CdS quantum dots (QDs) from root to shoot compared to the bare QDs in soybean.[55] In terms of surface charge, negative charges resulting from the coating facilitated NP transport in radish, ryegrass, rice, and pumpkin plants[60] and enabled faster transport of QDs in the conducting system of *Arabidopsis thaliana* compared to positively charged coatings.[61] In addition, organic polymers can provide steric stabilization for NPs,[62] which potentially plays an important role in stabilizing NPs under high salinity conditions.[63] Therefore, size and surface modifications could be employed to control the transport of NPs within plants.

In this study, we evaluated the effectiveness of NP delivery methods (foliar application, root application, branch feeding, and trunk injection) for citrus trees (Mexican lime and clementine mandarin *cv.* Nour grafted to Carrizo rootstock) and examined the fate and mobility of penetrated NPs. We used AgNPs in this study for three primary reasons: (i) AgNPs have a specific plasmonic and electronic signature that makes them easier to track in the complex plant matrix. (ii) Background Ag concentrations are relatively low, minimizing potential interference. (iii) AgNPs are known bactericides, making them attractive candidates for the treatment of citrus diseases, such as HLB. In addition, we studied the impact of size and surface coatings PVP, gum Arabic (GA), and sodium citrate (Ct)) on NP transport. Our results demonstrate that trunk injection can efficiently deliver NPs into trees, and NPs can move systemically both acropetally and basipetally through the tree's vascular system, with the majority of NPs remaining within the trunk. However, we cannot quantitatively differentiate the form of silver (*i.e.*, pristine NP, protein corona formation, silver ions, chelated ions, reprecipitated silver). Importantly, we tracked the flow of NPs from xylem to phloem (through the leaf), as well as potential excretion of NPs from the tree's roots. This study provides insight into the efficacy of a NP delivery method and the mobility of NPs in large, complex plants, such as trees.

https://dx.doi.org/10.1021/acsnano.9b07733
ACS Nano 2020, 14, 2966−2981

Table 1. Mean Concentrations of Inorganic Solutes Detected in Mexican Lime Leaf Sap

Inorganic Solutes (mM)								
K	Ca	Mg	Na	NH_4^+	NO_3^-	total N	P	S
104.7 ± 22.8	188.6 ± 65.6	38.3 ± 9.3	5.0 ± 1.3	9.0 ± 1.9	4.0 ± 0.7	67.1 ± 9.3	6.3 ± 2.4	16.4 ± 6.1
Cl	Si	Zn	Mn	B	Cu		Fe	
17.5 ± 4.9	1.1 ± 0.5	1.5 ± 0.1	0.5 ± 0.1	4.5 ± 1.4	0.1 ± 0.05		0.1 ± 0.08	

Table 2. Properties of AgNP with Different Surface Coatings[a]

surface modification	pristine size (*via* TEM, nm)	hydrodynamic diameter (nm)	ζ potential (mV)	surface concentration[d] (g/m^2)	layer thickness[e] (nm)
Ct	28.7 ± 11.0	94.3 ± 5.4[b]/428.2 ± 12[c]	−45.38 ± 3.84[b]/−4.24 ± 1.71[c]	9.6 ± 0.5 × 10^{-4}	negligible
PVP	17.9 ± 7.5	85.1 ± 3.6[b]/134.6 ± 2.5[c]	−32.29 ± 1.7[b]/−6.99 ± 0.28[c]	1.1 ± 0.1 × 10^{-3}	4.4
GA	9.2 ± 4.2	40.5 ± 1.3[b]/52.1 ± 8.9[c]	−32.76 ± 3.09[b]/−10.13 ± 0.63[c]	5.3 ± 0.7 × 10^{-2}	20.1

[a]Note: molecular weight of Ct, PVP, and GA (g/mol): 294, 40 000, and 250 000. [b]Measurements in nanopure water (pH 5.5, AgNP, 10 ppm). [c]Measurements in synthetic sap (pH 5.5; AgNP, 10 ppm). [d]Estimated from thermogravimetric analysis in the SI, Figure S4. [e]Detailed description on polymer layer thickness (in synthetic sap) estimation is provided in the SI, Figure S5. ($p > 0.05$, no significant difference among data from the same group).

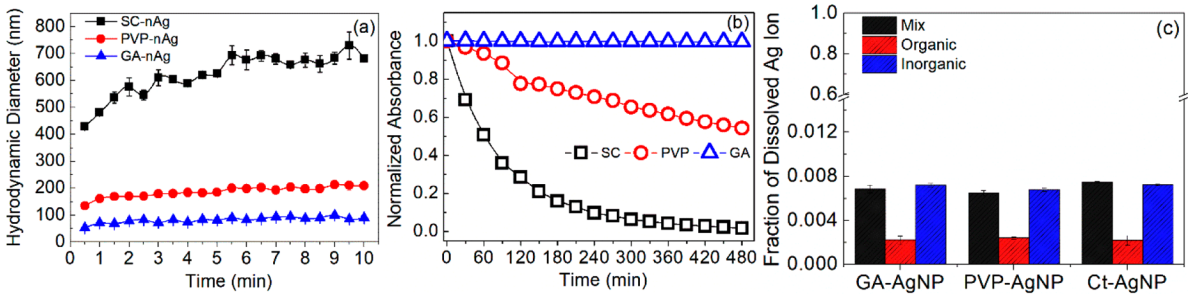

Figure 1. (a) Size evolution of AgNPs (10 ppm) in synthetic sap (pH = 5.5) within initial 10 min, (b) sedimentation of AgNPs (100 ppm) in synthetic sap (pH = 5.5), and (c) dissolution of AgNPs (100 ppm) in inorganic components of synthetic sap (Inorganic), organic components of synthetic sap (Organic), and synthetic sap (Mix) (pH = 5.5).

RESULTS AND DISCUSSION

Characterization of NPs in Synthetic Tree Sap. Because transport of NPs throughout the tree structure will likely involve movement through xylem and phloem, it is important to understand how NPs will behave in the sap that fills these vessels. We measured the concentrations of inorganic solutes in sap collected from the veins of Mexican lime leaves (the extraction process did not differentiate between xylem and phloem sap, and we did not identify organic compounds in the sap), and the result is shown in Table 1. Sap pH ranged between 5.5 and 5.9, with the most abundant cations being K^+ and Ca^{2+}. In terms of anions, Cl^-, SO_4^{2-}, PO_4^{3-}, and NO_3^- are the dominant species, which is in line with previous studies.[64,65] An examination of the concentrations in Table 1 reveals that (i) some of the Mg^{2+} and Ca^{2+} might form precipitates, and (ii) there is an imbalance between the total positive and negative charges in the sap, with an excess of positive charges being evident. It has been long recognized that a certain fraction of minerals exist as an insoluble form in synthetic sap,[66] and this fraction may vary from root to leaf and from day to night.[67] In addition, there are multiple organic species in citrus tree phloem sap, which consist primarily of sugars, short-chain carboxylic acids, and amino acids (Table S1).[37] We speculate that the mineral precipitates and the missing organic anions (*e.g.*, carboxylic acid groups) are responsible for the charge imbalance. The total ionic strength (associated with inorganic ions) of the sap was determined to be over 500 mM. The high salinity and abundant organics found in sap likely impact the aggregation, transport, and dissolution of NPs.[48]

The particle diameters of the synthesized PVP-, GA-, and Ct-AgNPs metal core, measured using transmission electron microscopy (TEM), were 17.9 ± 7.5, 9.2 ± 4.2, and 28.7 ± 11.0 nm, respectively (Table 2, Figure S1), while the hydrodynamic diameter (HD) of these NPs (Table 2) was 85.1 ± 3.6, 40.5 ± 1.3, and 94.3 ± 5.4 nm, respectively, in nanopure water. Each type of AgNP has a size distribution, which are statistically distinct (Figure S2a−c). Moreover, it is of great importance to characterize the NPs in aqueous conditions related to plant sap. On the basis of Table 1 and the literature,[66] we made a synthetic sap mainly consisting of dissolved species (conductivity, 29.33 mS/cm; ionic strength, 467 mM; total organic carbon, 1.60 ± 0.05 × 10^4 ppm; detailed composition could be found in Table S1). Once AgNPs were exposed to synthetic sap, the initial HD diameters of PVP-, GA-, and Ct-AgNP were 134.6 ± 2.5, 52.1 ± 8.9, and 428.2 ± 12 nm, and each AgNP still maintained a statistically distinct size range (Figure S2d−f) (correlograms for three dynamic light scattering, DLS, measurements are provided in Figure S3). Within 10 min, the size of GA-AgNP did not show significant change (89.8 ± 0.4 nm), while that of PVP-AgNP and Ct-AgNP increased to 208.7 ± 2.9 and 682 ± 12.4 nm, respectively (Figure 1a). This implies that GA successfully stabilizes the AgNP while citrate is not effective at AgNP stabilization in synthetic sap; PVP stabilizes the AgNP to a moderate extent. The similar ζ potential of the three types of AgNPs, as shown in Table 2 (PVP-, GA-, and Ct-AgNP: −6.99

https://dx.doi.org/10.1021/acsnano.9b07733
ACS Nano 2020, 14, 2966−2981

± 0.28, −10.13 ± 0.63, and −4.24 ± 1.71 mV), indicates that the high ionic strength of sap compresses the electrical double layer, which may limit the contribution of electrostatic repulsion to the stability of NPs in synthetic sap. Therefore, steric repulsion likely plays a critical role in NP stabilization. The Ct (molecular weight (M_w), 294 g/mol) coating provides the AgNP with carboxylate functional groups, which imparts additional negative charges to the NP surface. GA (M_w of 250 000 g/mol), a natural secretion from the Acacia tree, is an organic mixture consisting of 80 wt % polysaccharides (D-galactose, L-arabinose, L-rhamnose, D-glucuronic acid) and 20 wt % protein.[68] High concentrations of GA have been demonstrated to be able to stabilize emulsions in challenging aqueous conditions, with up to 25 mM $CaCl_2$.[69] PVP (M_w of 40 000 g/mol) is a nonionic polymer with C═O, C—N, and CH_2 functional group, containing a hydrophilic pyrrolidone moiety and a hydrophobic alkyl group. PVP coatings have been demonstrated to prevent NP aggregation through steric hindrance effects.[70] Using thermogravimetric analysis (TGA) and models of polymer layer thickness,[62,71,72] we estimated that the surface concentrations of Ct, PVP, and GA on AgNPs are $9.6 \pm 0.5 \times 10^{-4}$, $1.1 \pm 0.1 \times 10^{-3}$, and $5.3 \pm 0.7 \times 10^{-2}$ g/m^2, with PVP and GA forming a polymer layer with a thickness of 4.4 and 20.1 nm, respectively (a detailed description of how the polymer surface concentration and thickness were calculation is provided in the SI, Figures S4 and S5). Given that xylem pit membranes have pore diameters in the range 10−340 nm,[36,73−77] it is possible that pit membranes could block the transport of aggregated PVP- and Ct-AgNPs between xylem vessel elements. In terms of axial transport, as the average pores of phloem sieve plates and xylem perforation plates range between 200 nm and 1.5 μm,[36,73,74,78] these membrane-like structures do not impose significant size exclusion pressure on GA-AgNP transport but can stop the transport of most aggregated PVP- and Ct-AgNPs. However, single particles (nonaggregated), and in particular, smaller-sized GA-AgNPs, are likely to be able to travel through the pit membranes, which increases the overall conducting area available to these particles. In addition, it is worth noting that proteins in both xylem and phloem sap, especially sap from plants infected by pathogens or insects,[79,80] may displace the coatings on AgNPs and impact the fate and mobility of AgNPs in plants.[81] It is not clear if this is happening in our system and needs to be investigated in future studies.

To quantitatively explore the impact of size and ζ potentials on AgNP transport in conducting vessels, we employed the Derjaguin−Landau−Verwey−Overbeek (DLVO) model to calculate the interaction energy between NPs and the surfaces of the plant vascular system (xylem and phloem); a detailed description of DLVO calculations can be found in the SI. Our DLVO model shows that negative charges on PVP-, GA-, and Ct-AgNP surfaces result in repulsive interaction energies of 2.41, 2.29, and 3.58 kT, respectively. However, the sum of Lifshitz−van der Waals and electrostatic interaction energy of these three AgNP (both in xylem and phloem) is always negative, with large particle sizes resulting in high attractive forces between the NP and xylem/phloem surface (Figure S6). This suggests that electrostatic stabilization is not the main reason for NP stability, and there are other forces responsible for this stability that enables NP mobility in the vessels.

With a layer of PVP or GA out of AgNP, it is of great importance to take steric interaction into consideration for explaining mobility of NP in plants. It is assumed that the inner surface of xylem/phloem vessels is uncoated and flat, and the steric interaction (U_{ste}) consists of osmotic (U_{osm}) and elastic (U_{ela}) repulsive interactions (within a range of $0 < h < d$, where h is the distance between NP and vessel surface, and d is the layer thickness).[62] The osmotic and elastic interaction can be estimated through eqs 1−3:

$$U_{osm} = \frac{2\pi r\varphi^2 N_a}{V}\left(\frac{1}{2} - \chi\right)(d-h)^2 k_B T \quad (1)$$

$$\varphi = 3\frac{\Gamma_{max} r^2}{\rho[(d+r)^3 - r^3]} \quad (2)$$

$$U_{ela} = \frac{2\pi r\rho d^2 \varphi N_a}{M_w}\left[\frac{2}{3} - \frac{1}{6}\left(\frac{h}{d}\right)^3 - \left(\frac{h}{2d}\right) + \left(\frac{h}{d}\right)\ln\left(\frac{h}{d}\right)\right]k_B T \quad (3)$$

where r is the radius of NPs in synthetic sap derived from DLS intensity size (nm); φ, M_w, and ρ are the volume fraction, molecule weight (g/mol), and density (1.29 and 1.35 g/cm^3) of PVP or GA, respectively; N_a is Avogadro's number; Γ_{max} is the maximum surface concentration of PVP and GA; χ is the Flory−Huggins solvency parameter for GA (0.47) and PVP (0.45); T is temperature (K); and k_B is the Boltzmann constant. It is determined that once $h < d$, U_{ste} dominates the interactions between NPs and the xylem/phloem surface. This was particularly evident for the U_{ste} derived from GA modification, which was 2 orders of magnitude higher than the sum of the Lifshitz−van der Waals and electrostatic interaction energy (Figure S7). Therefore, it is very likely that repulsive steric interactions are the main reason for the mobility of NPs in plants.

While the impact of particle size, pH, temperature, natural organic matter, and common ions on AgNP dissolution has been well studied,[82−87] the dissolution of NPs in plant sap remains unknown. We investigated the dissolution of AgNPs in the following three types of media: (1) organic components of synthetic sap, (2) inorganic components of synthetic sap, and (3) synthetic sap (please refer to Table S1 for the detailed composition). It was found that after 7 days in all media ionic Ag accounted for less than 1% of total Ag, with the lowest ratio (0.22%) found in organic sap (Figure 1c). This value is far lower than the reported dissolution in deionized water (≫5%[82,85,87]), we employed UV−vis spectroscopy to investigate the composition of reacted AgNPs.[88,89] The results show that, indeed, the majority of AgNPs remained and that AgCl did appear in the reacted suspended solids derived from the reaction system with synthetic sap[90] (a detailed description on UV−vis spectra could be found in Figure S8). Since the ratio of dissolved Ag to total Ag in the inorganic sap solution and synthetic sap was very close (both were approximately 0.7%), it is likely that inorganic solutes present in sap accelerated the dissolution process of AgNPs, although relatively little dissolution took place. Based on a previous study,[43] the dissolution rate of AgNPs (average diameter of 32.9 nm) at a Cl/Ag molar ratio of 535 was 0.107 ± 0.020%/h, and an increase of the Cl/Ag ratio further increased the dissolution rate. However, in our study, while the Cl/Ag molar ratio was 610, and the size of AgNPs was smaller (both of which increase the dissolution rate), the dissolution rate declined. Thus, we conclude that the presence of organics in synthetic sap inhibited the dissolution of AgNPs,[91] which is in line with a previous finding that CeO_2 can transport from root to shoot

https://dx.doi.org/10.1021/acsnano.9b07733
ACS Nano 2020, 14, 2966−2981

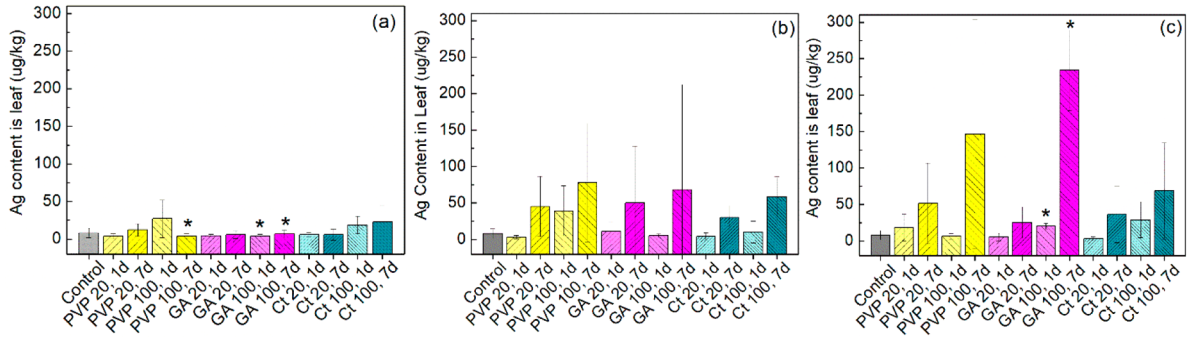

Figure 2. Average Ag content in six Mexican lime leaves (ranging from the closest to, to the farthest from (>50 cm) the dosing area) as a function of NP coating, suspension concentration, and time: (a) soil drenching; (b) foliar application; (c) branch feeding. (Control: no AgNPs exposure. 20 and 100: 20 and 100 ppm AgNP suspension. 1d and 7d: 1 day and 7 days postexposure. PVP, GA, and Ct: PVP-, GA-, and Ct-AgNP.) *, five samples were used for the plot as one sample was recognized as abnormal data in a box chart analysis. One-way ANOVA test plus Fisher's LSD test were used for statistical analysis ($p < 0.05$).

with very limited dissolution.[92] Since the antimicrobial properties of AgNPs are partly associated with their dissolution (as silver ions are responsible for the antimicrobial activity[93]), the slow dissolution of AgNPs in sap may reduce their antimicrobial performance, although it is unknown what concentration of silver ions is actually needed to induce a satisfactory antimicrobial response. However, this limitation can be potentially addressed by increasing the AgNP loading into the trees. Regardless, specific experiments regarding the efficacy of AgNPs as antimicrobial agents in trees are still needed.

Mobility of NPs Delivered by Different Methods. Soil drenching, foliar application (drop casting), and branch feeding were evaluated for their ability to deliver AgNPs into Mexican lime leaves. As demonstrated in Figure 2, the overall average Ag content (defined as mass Ag/mass of leaf tissue) was highest in leaves from plants exposed *via* the branch feeding treatment after 7 days (149.97 ± 82.70 μg/kg dry tissue), followed by that of plants exposed *via* foliar application (55.183 ± 17.10 μg/kg dry tissue) and soil drenching (13.95 ± 8.13 μg/kg dry tissue) (the difference between Ag content after 7 days in the branch feeding group and that in foliar application/soil drenching group is significant, while the difference in Ag content between the foliar application group and from the soil drenching group is not significant). The one-way analysis of variance (ANOVA) test plus Fisher's least significant difference (LSD) test indicated that the difference between the overall average Ag content from soil drenching group (9.97 ± 7.87 μg/kg) and the control (8.26 ± 6.45 μg/kg) was not significant, while the Ag content from branch feeding was significantly different from those in the control and soil drenching groups. However, the average Ag content in the branch feeding group (50.44 ± 67.39 μg/kg), while higher than that from foliar application group (31.78 ± 26.64 μg/kg), was not statistically significant. Our result thus implies that soil drenching is the least effective method for delivering NPs into leaves, which agrees with previous studies that reported that the majority of NPs applied to roots adsorb on their surfaces.[60,94−97] In the case of branch feeding, the average Ag content in leaves from PVP-, GA-, and Ct-AgNP fed trees was 58.71 ± 69.15, 71.48 ± 108.81, and 34.48 ± 27.05 μg/kg, respectively; these results are not statistically significantly different. However, based on the average values, it is likely that PVP and GA were more effective in enhancing NP transport, compared to Ct. Besides the smaller size of GA-AgNP and PVP-AgNP (than Ct-AgNP), the steric repulsion is regarded as the other important factor to the enhanced mobility of NP in plants based on our modeling work. In addition, while surface concentration of GA is much higher than that of PVP, the mobility of NPs in tree is not dramatically impacted by the identity of the coating. During our 7 day dissolution experiment in synthetic sap, we noticed that PVP-AgNP absorbed a considerable amount of organics from solution (possibly through the hydrogen bond due to the presence of abundant C═O groups[70]), but GA-AgNP and Ct-AgNP did not. It is possible that adsorbed organics from plant sap provide additional steric repulsion for PVP-AgNP. In terms of Ct-AgNP, citrate desorption can easily occur under high-salinity conditions,[98] and organics in sap, especially protein, probably can adhere to (*via* hydrophobic interaction) and thus stabilize some of the AgNPs,[99] contributing to the transport of Ct-AgNPs in tree. In general, increasing the transit time (interval between NP application and tissue harvesting) or NP dosage (from 20 to 100 ppm) resulted in a clear increase in Ag leaf content, suggesting that AgNPs were continuously transporting to leaves, and that higher AgNP loading resulted in higher Ag leaf content. However, based on other research,[100] a loading threshold can be reached, beyond which increasing NP concentrations does not necessarily result in an increase of leaf NP content; this may be due to the blockage of porous membrane structures' inhibition of NP transport between cells induced by NP aggregation.

We estimated the delivery efficacy of foliar application *via* dividing the Ag mass recovered from the whole tree with the total mass of Ag introduced (*i.e.*, dosed) to the tree, since these trees saw a substantially higher Ag leaf content compared to those exposed *via* soil drenching. Six weeks after foliar exposure (which had no adverse impact on plant growth), three trees (exposed to 0.5 mL of 100 ppm PVP-, GA-, or Ct-AgNP suspension) were destructively sampled and separated into leaf (did not include the original three leaves that had the AgNP dosage), branch, trunk, and roots. We recovered between 1.5 and 3.0 μg of Ag out of a total of 50 μg of Ag (the total mass of Ag added to the tree), accounting for 3−6% of the total applied AgNPs (Figure S9). This implies that AgNPs can transport to branch, trunk, and root from leaves through phloem, and that surface coating can impact the mobility of NPs in trees as the distribution of different types of AgNPs in leaves, trunk/branch, and root was different (Figure S9). In addition, it is possible that the delivery efficacy can be

https://dx.doi.org/10.1021/acsnano.9b07733
ACS Nano 2020, 14, 2966−2981

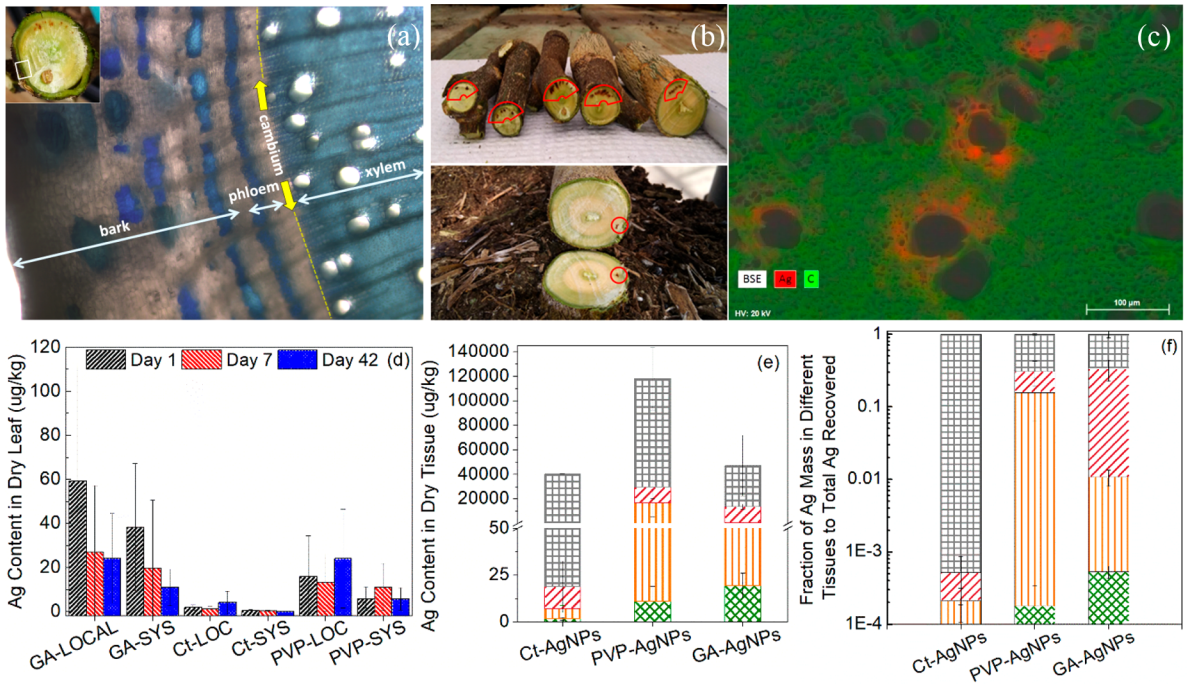

Figure 3. (a) Light microscope image of a cross-section of a mandarin tree trunk (insert is the photo of the cross-section of the trunk). (b) Trunk injection of GA-AgNPs (NPs are visible as brown staining in the secondary xylem tissue near the phloem (highlighted in red outline), and staining is always on the side of the trunk where the injection took place). (c) Elemental mapping of the brownish zone on the cross-section of the trunk by scanning electron microscopy with energy-dispersive X-ray spectrometry (color—element: green—carbon, red—silver). (d) Ag content in leaf material from trees injected with Ct-AgNPs, PVP-AgNPs, and GA-AgNPs on day 1, 7, and 42 postinjection (LOC and SYS: local leaves and systemic leaves). (e) Ag content in leaf, branch, trunk, and root recovered on day 42 postinjection. (f) Fraction of Ag mass in leaf, branch, trunk, and root to total Ag recovered on day 42 postinjection. (e and f: gray grid, trunk; red lines, root; yellow lines, branch; green grid, leaf) (10 mL of 1000 ppm AgNP, 2.5 year old clementine mandarin trees; one-way ANOVA test plus Fisher's LSD test were used for statistical analysis, $p < 0.05$).

higher because (i) the original leaf dosed with Ag was not included in the leaf sample, and (ii) tree roots are likely excreting NPs into the soil in a manner similar to wheat roots (more on this below).[98] Nevertheless, this rate is much higher than that of soil drenching, which has been reported to introduce between 0.03% and 0.11% of NPs into plants.[101,102] In foliar applications, a considerable amount of NPs can penetrate the plant through the stomata, without being trapped in the epidermis.[98] In contrast, the epidermis on the root blocks the majority of NPs from entering the plant, and an intact Casparian strip further prevents the apoplastic transport pathway of NPs.[28] It has been reported that foliar applications can deliver a larger amount of NPs into plant compared to soil applications.[14,20] However, in foliar applications, even for those NPs entering the plant through stomata, they still have to move through the mesophyll structure before reaching conducting vessels.[32] This mesophyll structure could possibly be a temporary storage place for NPs, hindering the transport of NPs to the phloem. However, in branch feeding, the AgNP suspension could be completely absorbed by the tree, allowing the direct flow of NPs from the feeding syringe to the phloem/xylem system. The method removes the hindrance of cuticle/epidermis/mesophyll structures to NP transport and can effectively deliver AgNPs into trees. However, during the feeding process, it was noted that the AgNP suspension uptake rate varied greatly from plant to plant (from 24 to 168 h), making this form of application difficult to implement. Therefore, we decided to explore trunk injection as a method to introduce 100% of NPs into plants within a shorter time frame.

In addition, it is worth mentioning that the difference in the initial conducting vessels the NPs encounter immediately after application could impact NP transport. Specifically, after foliar application (applied to the upper part of the tree) and branch feeding (at the tip of one branch), the main route of initial entrance would be through the phloem, while after trunk injection and soil application, it will likely be through the xylem. However, over the long-term, both xylem and phloem contribute to the transport of NPs within the tree.

Impact of Surface Coating on the Mobility of NP in Tree after Injection. In woody branches and trunks, a close proximity between the xylem and phloem is found just inside the bark (Figure 3a). In transverse sections, the xylem occupies most of the central cylinder of the stem all the way out to a ring of vascular cambium just beneath the bark. The cambium is a thin meristematic tissue that forms new xylem cells toward the inside of the limb, and new phloem cells toward the outside. The phloem occupies a very narrow zone just outside the cambium, and it is fragile. Therefore, delivery of NPs through trunk injection targets the xylem. 10 mL of a 1000 ppm AgNP suspension (Ct-AgNPs, PVP-AgNPs, GA-AgNPs) was injected into 2.5 year old clementine mandarin trees *via* trunk injection at 20−30 psi over a period of 2 h. On day 1, day 7, and day 42, three local leaves (*i.e.*, close to injection point) and three leaves from a point farthest away from the injection point (termed "systemic" leaves) were collected and measured for their Ag content. On day 42, trees were separated into leaf, branch, trunk, and roots and were destructively sampled with the goal of performing a mass balance on Ag and determining Ag distribution in the tree. Interestingly, after the

https://dx.doi.org/10.1021/acsnano.9b07733
ACS Nano 2020, 14, 2966−2981

trunk was cut into 4−5 segments (depending on total trunk length), multiple brown spots in the secondary xylem area were observed in successive segments in some of the trees, including in the segment below the injection point just above the roots (Figure 3b). This brown coloration demonstrates that trunk injection is able to deliver NPs throughout the trunk, including toward the roots. Furthermore, elemental mapping of the brownish zone on the cross-section of the trunk by scanning electron microscopy with energy-dispersive X-ray spectrometry confirms the appearance of AgNPs in xylem vessels, but not all xylem vessel elements (a small area along the trunk's secondary xylem) were used for NP transport (Figure 3c).

After injection, all three types of AgNPs move from the injecting point to leaves, but the surface coating impacted the transport process to different extents. Ag content in leaves from trees injected with GA-AgNPs ranked the highest, followed by trees injected with PVP-AgNPs, and then Ct-AgNPs (GA-AgNP group vs Ct-AgNP/PVP-AgNP group, $P < 0.05$; PVP-AgNP group vs Ct-AgNP group, $P > 0.05$), indicating that GA-AgNPs had the greatest potential for transport from trunk to leaf (Figure 3d). Of the trees receiving a GA-AgNP injection, Ag content in local leaves was always higher than that in systemic leaves, indicating possible transport restriction due to aggregation/deposition of AgNPs in xylem vessels, and possibly sieving imposed by the plant conducting system. Interestingly, in GA-AgNPs injected trees, both the local and systemic leaves exhibited the highest Ag content on day 1 (59.4 ± 52.5 μg/kg and 38.4 ± 28.9 μg/kg), declining to 27.01 ± 30.2 and 19.6 ± 31.11 μg/kg, respectively, on day 7 and to 24.15 ± 20.4 and 11.05 ± 8.2 μg/kg, respectively, on day 42 (Figure 3d) (day 1 local vs day 7/42 local, day 1 systemic vs day 42 systemic, $P < 0.05$). In addition, the changing Ag mass in leaves throughout the experiment (Figure S10) demonstrated a similar trend to that shown in Figure 3d. To estimate the possible contribution of biodilution to the change of Ag mass/content, we carried out Pearson correlations to quantify the possibility that high leaf weight could lead to high Ag mass in leaves (2-tailed test of significance was used). It was found that there was no significant correlation between them, indicating that biodilution may not be the main reason for the decline of leaf Ag mass/content. Therefore, the decline in mass over time implies that GA-AgNPs can transport within trees *via* both xylem (upward transport) and phloem (downward transport), and the downward transport may be removing AgNPs from the tree and into the roots. The decline of leaf Ag content was not apparent in trees injected with Ct-AgNPs and PVP-AgNPs, perhaps signifying that these NPs do not effectively move within plant. However, we cannot exclude the possibility that Ag mass/content change in local/systemic leaf could be impacted by (i) Ag^+ storage by proteins as a protection of the tree from the metallic contamination,[103] and (ii) a fraction of AgNPs being more mobile than others induced by a heterogeneity of NP coating density or sizes of the AgNP population.[104]

The distribution of Ag in injected trees on day 42 postinjection is shown in Figure 3e,f. For all three AgNP formulations, Ag content in the trunk was the greatest, followed by root, branch, and leaf. The Ag contents in the trunk from trees injected with Ct-AgNPs, PVP-AgNPs, and GA-AgNPs were 40 468.5 ± 224.1, 88 360.1 ± 25 429.7, and 33 394 ± 24 575.7 μg/kg (data collected in each set, $P > 0.05$), accounting for 99.9%, 69.0%, and 66.5% of the total mass of Ag recovered from the entire tree, respectively. These results demonstrate that Ct-AgNPs cannot efficiently transport within trees (likely due to their rapid aggregation in sap; although citrate on the NP surface can be readily replaced with macromolecules,[105] the contribution of this change to the mobility of Ct-AgNP is unclear). However, since PVP-AgNPs and GA-AgNPs resist aggregation, their continuous transport is enabled. While the Ag contents in roots from plants injected with PVP-AgNPs or GA-AgNPs were similar (12 941.9 ± 9125 vs 12 994.3 ± 2084.9 μg/kg, $P > 0.05$), Ag content in branches from plants injected with PVP-AgNPs (16 777.9 ± 11 254.4 μg/kg, $P > 0.05$) was much higher than that of trees injected with GA-AgNPs (735.2 ± 464.5 μg/kg, $P > 0.05$) (PVP-AgNP vs GA-AgNP, $P < 0.05$). In contrast, Ag content in leaves from plants injected with PVP-AgNPs (11.2 ± 7.9 μg/kg, $P > 0.05$) was slightly lower than that of trees injected with GA-AgNPs (19.4 ± 6.7 μg/kg, $P > 0.05$) (PVP-AgNP vs GA-AgNP, $P > 0.05$). Given the low Ag content found in leaves, the difference between these two coatings (on average 74% higher Ag content in leaves from trees injected with GA-AgNPs compared to those injected with PVP-AgNPs) implies that GA-AgNPs can transport to leaves more readily than PVP-AgNPs.

The delivery efficacy (*i.e.*, the mass of silver recovered from the tree after 42 days compared to the initial mass injected) of Ct-AgNPs, PVP-AgNPs, and GA-AgNPs *via* trunk injection was estimated to be 19.4 ± 2.3%, 39.5 ± 4.5%, and 22.8 ± 7.2%, respectively. Following the trunk injection, we observed small droplets containing Ct-AgNPs at the location of tree wounds (due to branch pruning) near the injection point; no such droplets were observed following the PVP-AgNP or GA-AgNP injection. Thus, not all of Ct-AgNPs were delivered into the trees, contributing to the low total Ag recovery (only ∼20% of Ag accounted for). Based on the relatively high transport of PVP-AgNPs and GA-AgNPs compared to Ct-AgNPs (*i.e.*, Ag content in the trunk from trees injected with Ct-AgNPs, PVP-AgNPs, and GA-AgNPs accounted for 99.9%, 69.0%, and 66.5% of the total mass of recovered Ag), and the large portion of Ag found in the roots, it is possible that these two types of NPs were excreted by the roots, suggesting that small NPs can be transported and excreted by plants more readily.[49] Therefore, it is hypothesized that root excretion contributes to the low recovery of Ag in trees that received PVP- or GA-AgNP injections.

Impact of Concentration on NP Transport Following Trunk Injection. GA-AgNPs exhibited the most robust transport behavior, moving from the trunk injection site to all parts of the tree. In particular, the higher mass of Ag found in the roots suggests possible AgNP transport between the xylem and phloem, though it is possible that the injection forces NPs into the root system itself. Thus, to further investigate AgNP transport during the first 7 days following injection, trees injected with a GA-AgNP suspension were destructively sampled on day 1, 3, and 7 and separated into leaf, branch, trunk, and root samples.

The distributions of Ag in the different tree segments on days 1, 3, and 7 postinjection with either 10 or 100 ppm GA-AgNPs are shown in Figure 4. The total Ag mass measured in the trees varied significantly between time-points, and no clear trend in Ag mass from day 1 to day 7 could be discerned. Among the trees injected with the 10 ppm GA-AgNP suspension, the total Ag mass recovered ranged between 14.2

https://dx.doi.org/10.1021/acsnano.9b07733
ACS Nano 2020, 14, 2966−2981

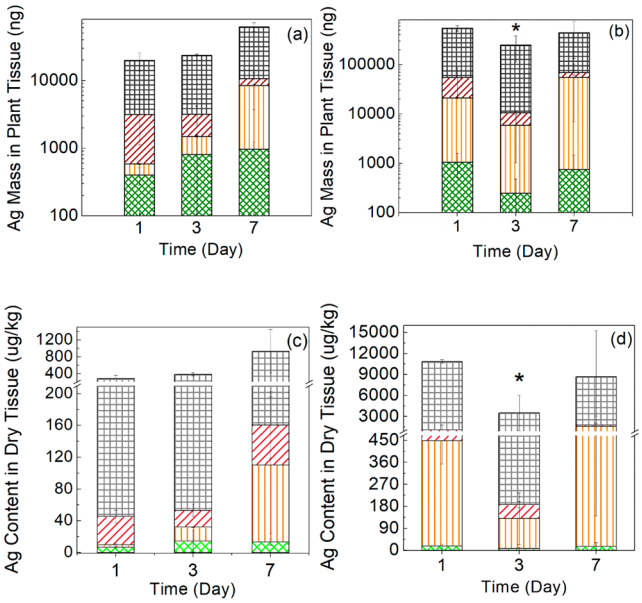

Figure 4. Ag mass recovered (a, b) and Ag content (c, d) in different tissues of 2.5 year old clementine mandarin trees injected with 10 mL suspensions of 10 ppm (100 μg Ag in total) (a, c) and 100 ppm (1000 μg Ag in total) (b, d) GA-AgNPs. Tissues were sampled on days 1, 3, and 7 after injection (gray grid, trunk; red lines, root; yellow lines, branch; green grid, leaf). *, injection of 100 ppm GA-AgNPs suspension on day 3 was not successful, and only 7 mL of suspension was injected within 2 h while the rest was 10 mL. (One-way ANOVA test plus Fisher's LSD test were used for statistical analysis ($P < 0.05$). Significant difference between the GA-AgNP group data and Ct-AgNP/PVP-AgNP group; no significant difference between the PVP-AgNP group and Ct-AgNP group.)

and 67.7 μg out of a total of 100 μg injected (Figure 4a), while that from trees injected with 100 ppm GA-AgNP suspension varied between 150.0 and 722.3 μg out of a total of 1000 μg injected (Figure 4b). In all cases, the vast majority (84.6 ± 3.4% of the total Ag recovered in trees injected with 10 ppm GA-AgNP suspension and 91.3 ± 5.5% in trees injected with 100 ppm GA-AgNP suspension) of the silver remained in the trunk over the 7 day experimental period. While the roots and branches had a considerable amount of Ag mass after injection, the total Ag mass in leaves remained small (<1.5 μg in both sets of injections), and the increase of concentration of the GA-AgNP suspension did not result in a proportional increase of Ag mass in leaves (Figure 4a,b). The total Ag mass in branches increased from 0.2 ± 0.01 to 7.5 ± 4.7 μg in trees injected with 10 ppm GA-AgNP suspension ($P < 0.05$), and from 20.1 ± 1.0 to 54.5 ± 48.3 μg in trees injected with 100 ppm GA-AgNP suspension ($P > 0.05$), as the harvesting time was extended from 1 day to 7 days. In contrast, Ag mass in roots declined slightly from 33.8 ± 33.4 to 13.5 ± 7.2 μg in trees injected with 100 ppm GA-AgNP suspension ($P > 0.05$), although this decline was not obvious in trees injected with 10 ppm GA-Ag NP suspension (2.6 ± 2.1 vs 2.3 ± 2.0 μg for days 1 and 7, respectively, *no significant difference*). That being said, (1) the increase of Ag mass in the branch from day 1 to day 7 may imply that GA-AgNPs were continuously transported to branches from the injection point, and (2) the decline of Ag mass in roots from day 1 to day 7 may imply that GA-AgNPs were excreted from the roots. In addition, the relatively constant Ag content in leaves from both groups with different injection concentrations might indicate a certain physiological response of the citrus tree to AgNPs (such as Ag detoxification and NP storage),[103] which needs to be more thoroughly investigated. However, the mass of silver we measured was highly variable within each group (evident by the large confidence intervals), making any conclusions highly speculative.

To further analyze the Ag distribution in the trees, we normalized the total Ag mass in different tree tissues with their dry weight (Figure 4c,d) and calculated the % mass of Ag in each tissue, relative to the total Ag mass recovered from the entire tree (Figure S11a,b). In Figure 4c, Ag leaf content increased from 6.6 ± 1.1 μg/kg on day 1 (% mass of Ag = 2.9%) to 14.3 ± 13.4 μg/kg on day 3 (% mass of Ag = 6.3%) before it slightly decreased to 13.3 ± 4.0 μg/kg on day 7, whereas the Ag content in roots declined from 35.8 ± 8.1 μg/kg (% mass of Ag = 19.0%) to 21.2 ± 7.6 μg/kg (% mass of Ag = 7.1%) from day 1 to day 3 before increasing to 50.4 ± 41.6 μg/kg (% mass of Ag = 8.9%) on day 7 (Figure 4c); the large confidence interval associated with the root content between trees reflects the large variability between sampled trees, which may be driven by natural physiological differences between trees. As the upward and downward transport of AgNP is responsible for the presence of Ag in leaves and roots, respectively, the dynamic variation of leaf and root content implies that the intensity of upward and downward transport is continuously changing. Similarly, in Figure 4d (trees injected with 100 ppm AgNP suspension), the overall average Ag content in leaf from the trees injected with a 100 ppm AgNP suspension was 13.5 ± 10.9 μg/kg (% mass of Ag = 0.1%), while that in trees injected with 10 ppm AgNP suspension was 11.0 ± 7.5 μg/kg (% mass of Ag = 3%) (Figure 4c) ($P > 0.05$). This suggests that the increasing concentration of AgNP suspension does not substantially increase the total amount of AgNPs in leaves. Seen in Figure 3c, AgNP transport does not occupy the entire xylem cylinder, which probably resulted from our single-point injection method. It is very likely that if the injection were extended to multiple points, the transport capacity of xylem for NPs could increase. In addition, on day 7, the Ag content in branches was higher (1584.0 ± 1459.5 μg/kg, % mass of Ag = 8.5%) than that on day 1 (430.8 ± 94.9 μg/kg, % mass of Ag = 3.7%) ($P < 0.05$), but the average Ag content in roots (205.4 ± 187.0 μg/kg, % mass of Ag = 3.7%) was lower than that on day 1 (673.4 ± 639.1 μg/kg, % mass of Ag = 5.2%) ($P > 0.05$) (Figure 4d). This suggests again that AgNPs were continuously transported to branches from the trunk *via* xylem vessels and were probably excreted out from the plant by the roots.

To verify whether AgNPs can indeed be transported downward through the phloem (eventually reaching the root) in trees with trunk injection, we measured Ag content in phloem-rich tissue (bark) and xylem-rich tissue (remaining tissue without bark) on the trunk 7 days after injection (from trees injected with 10 ppm AgNP suspension). While this is a rough estimate (*e.g.*, we cannot exclude the possibility that some xylem vessels remained attached to the bark), it helps illustrate the transport of NPs through the different plant conducting systems. It was found that the average Ag contents in xylem-rich and phloem-rich trunk tissue were 757.0 ± 512.0 and 300.5 ± 170.8 μg/kg (the injection was carried out in xylem-rich tissue) ($P < 0.05$), with the Ag content increasing from 154.2 ± 38.7 μg/kg in the top part of the phloem-rich trunk tissue (top 10 cm out of the total 20 cm long trunk) to

https://dx.doi.org/10.1021/acsnano.9b07733
ACS Nano 2020, 14, 2966−2981

Table 3. Pearson Correlation Coefficient (r) among Ag Mass in Leaf/Branch (μg), Ag Content in Dry Leaf/Branch (μg/kg), Dry Weight of Leaf and Branch (g), Total Length of Branch (cm), and Branch Distance from Injection (cm) (Samples from Clementine Mandarin Trees Received 10 or 100 ppm GA-AgNP Injection)

index	Ag mass in leaf[a]	leaf Ag content[a]	Ag mass in branch[a]	dried branch weight[a]	Ag content in branch[a]	total length of branch[a] (cm)	branch distance from injection (cm)
dried leaf weight[a]	0.094	−0.23	−0.057	0.609[b]	−0.196	0.715[b]	0.361[b]
Ag mass in leaf[a]		0.916[b]	0.35[b]	−0.006	0.343[b]	−0.133	−0.086
leaf Ag content			0.399[b]	−0.18	0.427[b]	−0.336[b]	−0.216
Ag mass in branch[a]				0.277[c]	0.958[b]	−0.044	−0.195
dried branch weight[a]					0.042	0.737[b]	0.078
Ag content in branch						−0.242[c]	−0.195
total length of branch							0.187

[a]One branch or in a few cases two branches located close to each other on the trunk were grouped, and leaves in the same group of branches were classified into one sample. [b]Correlation is significant at the $p = 0.01$ level. [c]Correlation is significant at the $p = 0.05$ level.

446.8 ± 19.3 μg/kg in the bottom part of the phloem-rich trunk tissue (bottom 10 cm out of the total 20 cm long trunk) ($P < 0.05$). This indicates that AgNPs were continuously transporting from trunk to root *via* phloem,[51,52] although we cannot rule out radial transport of NPs between the xylem and the phloem, driven by damage to the vessels sustained during the injection process.

In an effort to understand the distribution of AgNPs in the root system, we separated the main roots from the root hairs and measured their Ag content. For trees injected with the 10 ppm AgNP suspension, the average Ag contents in the main roots and root hairs were 34.4 ± 10.1 and 55.5 ± 3.0 μg/kg, respectively ($P < 0.05$); for trees injected with the 100 ppm AgNP suspension, the average Ag content in the main roots and root hairs was 219.2 ± 61.8 and 49.5 ± 33.7 μg/kg, respectively ($P < 0.05$). The high Ag content in the root hairs (which was usually higher than that in leaves and some branches) suggests that phloem conveys AgNPs from the main root to root hairs, where AgNPs are likely excreted out from the tree, in a process similar to plant sugar, amino acid, organic acid, nucleotides, and enzyme secretion.[106−108] While this conclusion is speculative, a recent study has shown that gold NPs are excreted by wheat roots, when the NPs were applied *via* a foliar application.[49]

In our study, as direct phloem delivery is impracticable, the xylem is the primary target for delivery of NPs during injection. However, the appearance of AgNPs in trunk phloem and root implies the potential application of nanotechnology for CLas growth control. This is because the CLas bacteria, phloem-resident, move down to the roots and multiply although they enter the plant by insects feeding on the phloem of aerial tissues (leaves, branches).[109]

Influence of Plant Structure on the Transport of AgNPs from Trunk to Leaf. In the present study, we found that Ag content in different leaves from different branches varied significantly, and we hypothesized that a high AgNP content (μg Ag/kg dry tissue) in a branch will result in a high AgNP content in leaves on this branch. To test this hypothesis, we determined the correlation between dried leaf weight (g), Ag mass in leaves (μg of Ag recovered), Ag content in leaves (μg Ag/kg dry leaf), the Ag mass in a branch (μg of Ag recovered), Ag content in a branch (μg Ag/kg dry branch), dried branch weight (g), branch length (cm), and the distance of the branch from the injection point (cm) using Pearson's correlation analysis. We did not find significant correlation between "dried leaf weight" and "Ag mass in leaf" or "Leaf Ag content", indicating that leaf development does not significantly impact the transport of AgNPs into the leaf (in other words, biodilution is not likely the main reason for the decline of Ag content in leaf observed from the tree study). However, we do find that the Ag content in leaves was positively correlated with the Ag mass/content in a branch ($r > 0.34$, $p = 0.01$) (Table 3). In addition, Ag content in leaves was negatively correlated with the total length of the branch ($r = −0.336$, $p = 0.01$), while the negative correlation between Ag mass in leaves and total length of branch was not significant (Table 3). This implies that a higher AgNP content in a branch yields higher AgNP content in leaves, and a longer branch reduces the mass of Ag in leaves. That is to say there is a physical process (*i.e.*, crossing through the pit membrane) reducing the mobility of NPs with longer transport distances. Moreover, as seen from Table 3, the AgNP mass in a branch is positively correlated with the dry weight of the branch ($r = 0.277$, $p = 0.05$), and possibly negatively correlated with total length of branch (although the correlation is not significant). Thus, it is likely that a short branch with a large diameter facilitates NP transport from trunk to leaf. In addition, as seen from Figure 3, since not all the xylem vessels are used for AgNP transport, branches that happen to be connected to the vessels which convey AgNPs will likely have higher AgNP content.

The total amount of Ag recovered in the 14 clementine mandarin trees (receiving 10 or 100 ppm GA-AgNP suspension injection) studied in the mass-balance experiments ranged between 14.22% and 72.23% of the total Ag mass injected (Figure S12). Interestingly, the low recovery (<30%) was often associated with high dry weight of root (>60 g dry weight, for 2−3 years old clementine mandarin trees) or a high weight ratio of root to the whole tree (>0.25) while the high recovery ratio (>45%) was related to a low dry weight of root (<60 g dry weight, for 2−3 years old citrus trees) or a low weight ratio of root to whole tree (<0.25). This further strengthens our hypothesis that AgNPs can be excreted by citrus roots, with larger root systems capable of faster excretion.

Tracking AgNPs in Leaf Tissue. To confirm the appearance of AgNPs on leaf, the midrib area from a systemic leaf collected from a clementine mandarin tree 1 day after a 10

https://dx.doi.org/10.1021/acsnano.9b07733
ACS Nano 2020, 14, 2966−2981

mL 100 ppm GA-AgNP suspension injection was isolated, embedded, and microtomed for scanning transmission electron microscopy (STEM) analysis. It was confirmed that AgNPs were present in xylem vessels (Figure 5a), made evident by the

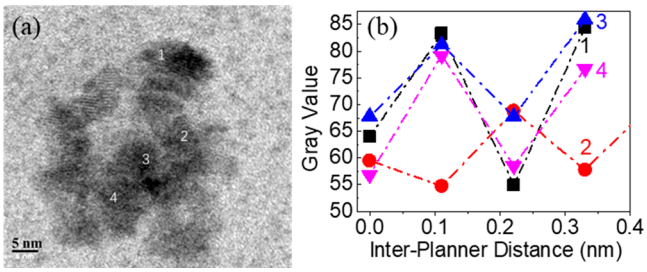

Figure 5. (a) NPs (darker region of TEM image) found in the xylem of a systemic leaf collected 1 day after a 10 mL 100 ppm GA-AgNP suspension injection, and (b) lattice space profile of the particles (the average lattice space calculated from areas 1, 2, 3, and 4, d = 0.23 nm).

their particle lattice spacing profile, calculated to be 0.23 nm, which matches the spacing of the (1, 1, 1) crystallographic plane of AgNPs (Figure 5b).[110] Additional STEM/TEM results showing AgNPs in leaf samples (xylem area, membrane, or extracellular spaces) are provided in Figure S13.

To further explore the transport pathway of AgNPs on leaf, a 20 cm branch from a clementine mandarin tree was placed into a 100 ppm GA-AgNP suspension for 24 h (in which way we can increase the amount of AgNPs on leaf significantly, further enabling us to identify a possible AgNP transport pathway on leaf through microscopic hyperspectral imaging). A leaf on the tip was collected, and the midrib area was isolated, embedded, and microtomed. AgNPs were identified within leaves using hyperspectral imaging, which enabled us to compare the relative abundance of AgNPs in different locations. It was found that there were likely more AgNPs in the extracellular space than the intracellular spaces of palisade and mesophyll cells near the stomata area (area St, Figure 6a,b). However, hyperspectral imaging is a semiquantitative analysis method (as most microscopy methods are), and these results must be considered in this context. In addition, we observed AgNPs in both the extracellular and intracellular spaces of bundle sheath cells, as well as in the intracellular spaces flanking phloem elements (areas Ph and Bs, Figure 6c,d and Figure S14). Interestingly, few AgNPs were found in the xylem. Therefore, we speculate that AgNPs move apoplastically from the xylem to the stomatal region *via* mesophyll cells due to evapotranspiration. Coincidently, assimilated sugars from photosynthesis in mesophyll cells continuously diffuse into the phloem, and these accumulated sugars draw water (osmotically) from the adjacent xylem into the phloem.[111,112] Thus, the NPs are advected into the phloem along with the water.[32] However, it must be acknowledged that the NP transport pathway identified using hyperspectral image analysis may not fully represent the movement of NPs in leaves from the citrus tree injected with AgNPs, as the density of NPs in the leaf from the cut branch was much higher, and we did not take the physiological response of the leaf in response to its pruning into consideration.

CONCLUSION

In the present study, we demonstrate that trunk injection, among the four methods tested for the delivery of AgNPs into trees (other delivery methods tested were foliar application, branch feeding, and soil drenching), can readily deliver a large amount of AgNPs into citrus trees. After delivery, Ct-AgNPs tend to stay within the trunk because of the fast aggregation induced by the high salinity of the sap, while PVP- and GA-AgNPs can be distributed throughout the whole tree *via* both upward and downward transport due to the strong steric repulsion resulting from the surface coating. We demonstrate that the root system could be a sink of NPs as a considerable

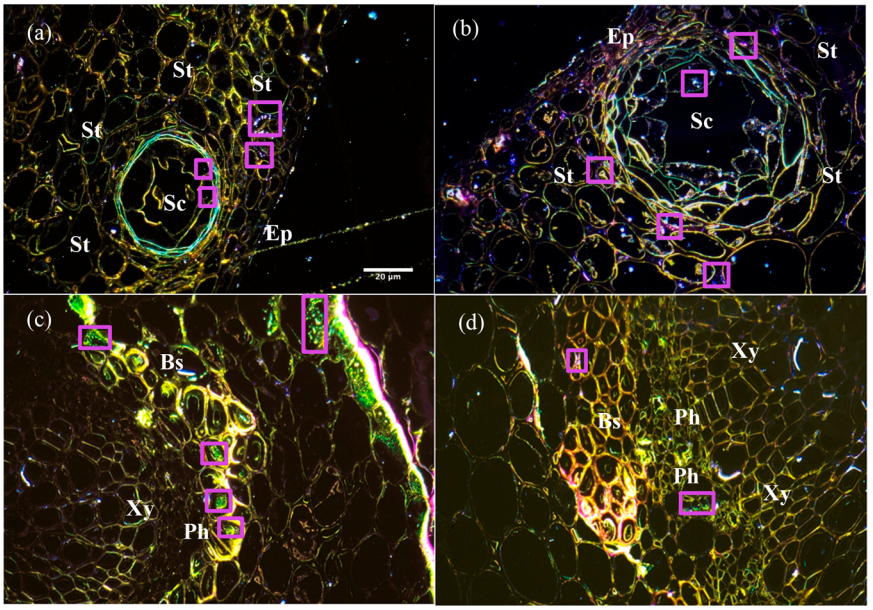

Figure 6. Hyperspectral image analysis of the AgNP distribution in a microtomed midrib of a clementine mandarin leaf (detected AgNPs shown in purple rectangles) obtained by immersing a 20 cm branch into a 100 ppm GA-AgNP suspension for 24 h: (a, b) stomatal area; (c, d) xylem/phloem/bundle sheath areas. The different leaf components, epidermis, substomatal cavity, spongy tissue, xylem, phloem, and bundle sheath are labeled as Ep, Sc, St, Xy, Ph, and Bs, respectively. The scale bar in part a applies to all panels.

https://dx.doi.org/10.1021/acsnano.9b07733
ACS Nano 2020, 14, 2966−2981

amount of AgNPs were found there, and in addition, root hairs likely excrete NPs out from the tree. In terms of transport of AgNPs from trunk to leaves, short branches close to the injecting point tend to have a high Ag content, which leads to high Ag content in leaves on these branches. Moreover, on leaves, a potential transport pathway of AgNPs from xylem to phloem near stomatal areas was identified. This study shows the potential of using NPs as antimicrobial agents or gene delivery vehicles in perennial tree crops.

METHODS

Materials. Sodium citrate, polyvinylpyrrolidone (PVP, M = 40 000), gum Arabic (GA, M = 250 000), silver nitrate solution (0.1 M), sodium borohydride, $MgSO_4$, NH_4NO_3, KCl, $CaCl_2$, $MgCl_2$, NaCl, boric acid, $Fe(NO_3)_3$, $ZnSO_4$, $CuCl_2$, KH_2PO_4, fumaric acid, malic acid, proline, sucrose, glucose, fructose, citric acid, quinic acid, asparagine, glutaraldehyde, nitric acid, and hydrochloric acid were purchased from Sigma-Aldrich and used without further modification. Embed 812 resin was bought from Fisher.

AgNP Synthesis. AgNPs were synthesized according to a previous study.[113] Briefly, 10 mL of $AgNO_3$ stock solution was added into 270 mL of nanopure water. Then, 10 mL of GA (10 wt %), PVP (10 wt %), or sodium citrate (10 wt %) was added, and the solution was stirred at 1000 rpm for 15 min in an ice bath. Sodium borohydride (10 mL, 1 wt %) solution was then added, and the mixture was further stirred for an additional 1 h (in an ice bath). Vacuum filtration (PS 35 membrane, Solecta, Oceanside, CA; at 50 psi) was used to separate the NPs from the aqueous media, followed by a triple wash with nanopure water. AgNPs deposited on the membrane were then collected, used to make a 1000 ppm aqueous suspension, and kept in a refrigerator (4 °C).

Plant Material. Two different citrus species were used to study AgNP *in planta*: (1) 2−3 year old Mexican lime (*Citrus aurantifolia* (Christm.) Swingle) growing in a greenhouse at UC Riverside in 2017, and (2) 2−3 year old clementine mandarins (*Citrus clementina* hort. ex Tanaka) grafted to Carrizo rootstock (*Citrus sinensis* (L.) Osbeck × *Poncirus trifoliata* (L.) Raf.) growing in the same UC Riverside greenhouse in the spring (26 February to 20 March) and fall (11 September to 5 November) of 2018. All citrus plants were hand-watered using tap water or fertilizer water (a NPK 21:5:20 mix). Temperature control in the greenhouse consisted of a 3-stage cooling system, with an exhaust fan set to turn on at 85 °C, followed by a blower and an evaporative cooler once 89 °C is reached.

NP Characterization (Aggregation and Dissolution Analysis). 2−3 year old Mexican lime was used for all AgNP delivery and transport studies. Leaves were collected on May 5, 2016, and May 12, 2017 (ten leaves from each tree in duplicate), and were immediately sent to Cal G.A.P. Inc. (NovaCropControl, Netherlands) for sap extraction and inorganic solutes analysis.[114] Based on this analysis and a recent study,[37] synthetic citrus sap was composed of 995 mM KCl, 90 mM $CaCl_2$, 20 mM $MgCl_2$, 5.0 mM $NaNO_3$, 6 mM KH_2PO_4, 65.9 mM sucrose, 20.5 mM glucose, 10.3 mM fructose, 55.1 mM malic acid, 28.2 mM citric acid, 68.0 mM proline, and 16.6 mM asparagine into deionized water, with the pH adjusted to 5.5 with 0.1 NaOH and 0.01 M HCl. The inorganic sap solution contained only the inorganic solutes, while the organic sap solution contained only the organic solutes in the synthetic sap. PVP-, GA-, and Ct-AgNPs (10 ppm; prepared from the AgNP stock suspension) were used for HD size and ζ potential measurements using a ZetaPlus instrument (BrookHaven). To measure the ζ potential of AgNP in synthetic sap accurately, we conditioned the electrode before measurement (detailed information could be found in the SI). Aggregation of AgNPs was continuously monitored *via* changes in the HD measured every 30 s over a period of 10 min. Sedimentation tests were carried out on UV−vis spectrometry (Thermo Scientific Evolution 350) by measuring absorbance at 395 nm every 30 min over a period of 8 h. Dissolution tests were carried out in 12 mL glass vials with a PTFE cap (Fisher Scientific). Synthetic inorganic sap, organic sap, or sap (10 mL), containing 100 ppm AgNPs, was added into the vials. After 7 days, ionic Ag concentrations in each vial were measured using ICP-MS (NexION 2000, PerkinElmer, with detection limit, 0.2 ppb) after the vials underwent centrifugation at 25 000g for 60 min (Sorvall, Thermo Scientific), filtration through a 0.22 μm polyvinylidene fluoride filter, and acidification in 5% of nitric acid (control experiments with fresh Ct-, PVP-, and GA-AgNP in these aqueous media confirmed that centrifugation and filtration can successfully separate AgNPs from the media).

AgNP Uptake and Transport in Mexican Lime Plants after Foliar Application, Soil Drenching, and Branch Feeding. Suspensions of 20 ppm (0.5 mL, 10 μg) and 100 ppm (0.5 mL, 50 μg) PVP-, GA-, and Ct-AgNPs were applied to Mexican lime trees *via* foliar application, soil drenching, and branch feeding (Figure S15a). In the foliar application, three well-developed leaves (on the same branch, top of the tree, about 75 cm above the soil) were gently abraded with fine sandpaper, and 0.17 mL of solution was added to each of the three leaves (0.5 mL total). In the soil drenching, a small amount of topsoil (3 cm below the base of the trunk) was removed to expose roots, and then, a 0.5 mL AgNP suspension was dripped onto the roots, which were covered back up afterward. In branch feeding, the tip of a branch (length, over 35 cm; height, >15 cm above soil) was cut, and a 5 mL syringe was connected to the cut branch with rubber tubing and sealed with silicon tape. A 0.5 mL solution was added into the syringe and, through gravity, was allowed to be absorbed by the plant. On 1 day and 7 days after NP exposure, 6 leaves were collected for Ag analysis. The leaf samples were dried at 80 °C for 48 h. After the dry weight was measured, leaf samples were combusted (at 550 °C), and the ash was collected and digested with aqua regia (at 110 °C for 1 h). Ag concentrations were measured by ICP-MS. After 6 weeks, six trees exposed through foliar application (2 trees for each type of AgNP application) were sacrificed and separated into leaves (those remaining after sampling on day 1 and day 7), branches, trunk, and roots. Ag content in these tissues was analyzed, and the total mass of Ag in the trees was obtained.

AgNP Transport in Clementine Mandarin Trees Following Trunk Injection. AgNP suspensions were injected into clementine mandarin trunks (~5 cm above the soil; diameter of injection whole, ~1 cm) using a pneumatic injection instrument (Figure S15b). Injections were performed at a pressure of 20−80 psi. While the majority of injections were completed within 2 h, two injections with the GA-AgNP suspension required up to 24 h to complete; it is not clear why certain injections required longer times. However, it is unlikely that xylem blockage is responsible for the longer injection times, since the rapidly aggregating Ct-AgNPs never took more than 2 h to inject. Two rounds of experiments were conducted. First, to test the impact of surface modification on AgNP transport, 10 mL of 1000 ppm (10 mg Ag in total) Ct-, PVP-, and GA-AgNP suspensions was injected into trees (three trees for each modification type of AgNPs) (starting from 02/26/2018). Three local (near the injection point) and 3 systemic (farthest away from the injection point) leaves were collected on day 1, 7, and 42 postinjection. On day 42, trees were separated into leaves, branches, trunk, and roots for Ag mass distribution and mass balance analyses. Second, to examine the impact of AgNP concentration on NP transport in trees (postinjection), 10 mL of GA-AgNP suspensions (10 and 100 ppm, 0.1 and 1 mg of Ag in total) was injected into a total of 18 trees (three replicate injections of three trees at each AgNP concentration) (starting from 09/17/2018). On day 1, day 3, and day 7 postinjection, trees were separated into leaves, branches, trunk, and roots. In general, the trunk was cut into 3−5 pieces, and 4−7 branches were sampled, noting the distance between the point of branch insertion on the trunk and the injection point. Leaves from the same branch were collected together. To verify the appearance of AgNPs in phloem-rich tissue, we carefully peeled the tissue located outside of the cambium layer (mainly bark and phloem illustrated in Figure 3a), and the rest of the peeled trunk was xylem-rich tissue. In addition, we also separated the root hairs from main root for quantifying Ag mass in root hairs. All plant tissues were weighed after drying at 80 °C for 48−72 h (until the weight stopped changing) and then combusted at 550 °C. The ash was recovered and digested using aqua regia (at 110 °C for 1 h). Ag concentrations in

https://dx.doi.org/10.1021/acsnano.9b07733
ACS Nano 2020, 14, 2966−2981

the digested ash were measured using ICP-MS. To test the reliability of the analytical method, a 10 μL drop of 100 ppm AgNP suspension was placed onto three leaves, three segments of trunk, and the main root (from a tree that was not injected with AgNPs). After incineration and acid digestion, we recovered between 95% and 98% of the total Ag added, demonstrating the robustness of the analysis.

Visualizing GA-AgNPs in Clementine Mandarin Branch and Leaves. To confirm the transport of GA-AgNPs from injection point to branch, short branch sections were removed at a distance of about 2 cm above the injection point and cut to a length of 1 cm using a low-speed diamond wheel saw model 650 (South Bay Technology, Inc., San Clemente, CA). The surface was polished with a glass knife installed on an RMC MT-X microtome (Boeckeler Instruments, Inc., Tucson, AZ). Electron microscopy and EDX microanalysis were performed on a Tescan Mira3 SEM instrument (Tescan, Brno, Czech Republic) equipped with a Bruker Quantax EDS system (Bruker, Billerica, MA) in the Central Facility for Advanced Microscopy and Microanalysis (CFAMM) at University of California at Riverside.

To explore the transport of AgNPs from the injection point to leaves, systemic leaves were collected 1 day following a 100 ppm GA-AgNP suspension injection. A 2 × 3 cm leaf tissue sample (midrib area close to petiole) was cut and fixed in 5% glutaraldehyde for 24 h at 4 °C. The sample was then washed three times with a 0.1 mol/L pH = 7.2 phosphate buffer and dehydrated with a series of graded acetone (10%, 30%, 50%, 70%, 90%, and 100%). Then, the tissue was embedded in epoxy resin (ETON 812).[115] The embedded samples were microtomed (Leica) into 200 nm slices using a diamond knife onto a standard microscope slide (fixing, embedding, and microtoming were carried out in the Pathology and Laboratory Medicine department, University of California at Los Angeles). The slide was then sent to Duke University and imaged using a hyperspectral microscope (CytoViva, Auburn, Al). After CytoViva analysis, an area of sample determined to contain AgNPs was chosen and was sectioned to 60−80 nm for both TEM (T12 cryo-electron microscope, FEI Tecnai) and STEM (Titan 80-300 kV, FEI) analyses.

To investigate AgNP transport between the xylem and phloem near and around the stomatal openings on the leaves, we used hyperspectral imaging to identify AgNPs throughout the leaf structure. A 20 cm branch (with 10 leaves) was cut and placed in a 100 ppm GA-AgNP nanopure water suspension. After 24 h, a leaf from the top of the branch was collected, and the leaf blade was embedded and microtomed to 200 nm thick sections and imaged using hyperspectral microscopy. A reference spectral library consisting of 38 spectra was manually constructed from a control sample of 5 mg/L GA-AgNP in nanopure water (Figure S16), which was allowed to settle onto the glass surface overnight. Manual selection of spectra was performed in order to ensure high-quality, representative spectra while minimizing the probability of false positives. Matching of the reference library to treated and control leaf samples was conducted using the spectral angle mapping method with a threshold of 0.25 rad, thus revealing individual and clustered AgNPs within samples. This resulted in a false positive rate in control leaf samples of <0.005% by number of pixels (~5 pixels/image), while positively matching >75% of particles in control AgNP images. Detection in a AgNP-treated sample was considered positive when at least 0.5% of pixels in the image matched the spectral library to the same 0.25 rad threshold. Any spectra which consistently resulted in false positives were removed from the spectral library during the optimization process. Additional images showing mapped pixels in treated and negative control tissues are provided in the SI, Figure S17.

Statistical Analyses. All the data were presented as mean ± SD (standard deviation). We performed a one-way ANOVA test plus Fisher's LSD test for statistical analysis. $p < 0.05$ was considered to be significant.

ASSOCIATED CONTENT

Supporting Information

The Supporting Information is available free of charge at https://pubs.acs.org/doi/10.1021/acsnano.9b07733.

Derjaguin−Landau−Verwey−Overbeek (DLVO) model description; polymer layer thickness estimation; electrode conditioning for ζ potential measurement; TEM images; size distribution; correlograms; average weight change vs temperature; electrophoretic mobility; DLVO interaction energy profile; classic DLVO and steric interaction energy; UV−vis spectra; Ag mass recovered; relationships between Ag mass recovery ratio and dry root weight; CytoViva analyses; branch feeding and trunk injection; hyperspectral images and corresponding dark field images; and synthetic sap composition of Mexican lime (PDF)

AUTHOR INFORMATION

Corresponding Author

David Jassby − *Department of Civil and Environmental Engineering, University of California, Los Angeles, California 90095, United States;* orcid.org/0000-0002-2133-2536; Email: jassby@ucla.edu

Authors

Yiming Su − *Department of Civil and Environmental Engineering, University of California, Los Angeles, California 90095, United States;* orcid.org/0000-0001-6035-7384

Vanessa E. T. M. Ashworth − *Department of Botany and Plant Sciences, University of California, Riverside, California 92521, United States*

Nicholas K. Geitner − *Department of Civil and Environmental Engineering, Duke University, Durham, North Carolina 27708, United States;* orcid.org/0000-0003-4313-372X

Mark R. Wiesner − *Department of Civil and Environmental Engineering, Duke University, Durham, North Carolina 27708, United States;* orcid.org/0000-0001-7152-7852

Nichole Ginnan − *Department of Plant Pathology, University of California, Riverside, California 92521, United States*

Philippe Rolshausen − *Department of Botany and Plant Sciences, University of California, Riverside, California 92521, United States*

Caroline Roper − *Department of Plant Pathology, University of California, Riverside, California 92521, United States*

Complete contact information is available at: https://pubs.acs.org/10.1021/acsnano.9b07733

Author Contributions

Y.S., M.W., P.R., C.R., and D.J. designed research. Y.S., V.E.T.M.A., N.K.G., and N.G. performed research. Y.S., V.E.T.M.A., N.K.G., and N.G. contributed new reagents/analytic tools. Y.S., V.E.T.M.A., N.G., and D.J. analyzed data. Y.S., V.E.T.M.A., M.W., P.R., C.R., and D.J. wrote the paper. All authors have given approval to the final version of the manuscript.

Notes

The authors declare no competing financial interest.

ACKNOWLEDGMENTS

This work was financially supported by the United States Department of Agriculture (CA-R-PPA-5139-CG). We acknowledge the kind help from Dr. Ryan K. Thor on fixing,

embedding, and microtoming the leaf sample, Dr. Jared Lodico on STEM operation, and Dr. Chonghyun Chang on ICP-MS analysis and ultracentrifuge and acknowledge the use of ICP-MS facility within the UC Center for Environmental Implications of Nanotechnology in CNSI at UCLA.

REFERENCES

(1) Lin, B. *Fruit and Vegetable Consumption Looking Ahead to 2020*, Agiculture Information Bulletin 792-7; USDA: Washington, DC, 2004.
(2) United States Department of Agriculture. *2019 Farm Sector Income Forecast*. https://www.ers.usda.gov/topics/farm-economy/farm-sector-income-finances/farm-sector-income-forecast/ (accessed 11/27/2019).
(3) Siegel, K. R.; Ali, M. K.; Srinivasiah, A.; Nugent, R. A.; Narayan, K. M. V. Do We Produce Enough Fruits and Vegetables to Meet Global Health Need? *PLoS One* **2014**, *9*, No. e104059.
(4) Alvarez, S.; Rohrig, E.; Solís, D.; Thomas, M. H. Citrus Greening Disease (Huanglongbing) in Florida: Economic Impact, Management and the Potential for Biological Control. *Agric. Res.* **2016**, *5*, 109−118.
(5) Grafton-Cardwell, E. E.; Stelinski, L. L.; Stansly, P. A. Biology and Management of Asian Citrus Psyllid, Vector of the Huanglongbing Pathogens. *Annu. Rev. Entomol.* **2013**, *58*, 413−432.
(6) Iftikhar, Y.; Rauf, S.; Shahzad, U.; Zahid, M. A. Huanglongbing: Pathogen Detection System for Integrated Disease Management − A Review. *J. Saudi Soc. Agric. Sci.* **2016**, *15*, 1−11.
(7) Young, P. M.; Hutchins, A. S.; Canfield, M. L. Use of Antibiotics to Control Bacteria in Shoot Cultures of Woody Plants. *Plant Sci. Lett.* **1984**, *34*, 203−209.
(8) Compant, S.; Duffy, B.; Nowak, J.; Clement, C.; Barka, E. A. Use of Plant Growth-Promoting Bacteria for Biocontrol of Plant Diseases: Principles, Mechanisms of Action, and Future Prospects. *Appl. Environ. Microbiol.* **2005**, *71*, 4951−4959.
(9) Rani, A.; Singh, R.; Kumar, P.; Singh, C. Nanotechnology: An Emerging Strategy against Phyto-Pathogens in Agricultural Crops. *Adv. Life Sci.* **2015**, *4*, 35−37.
(10) Zhang, H.; Demirer, G. S.; Zhang, H.; Ye, T.; Goh, N. S.; Aditham, A. J.; Cunningham, F. J.; Fan, C.; Landry, M. P. DNA Nanostructures Coordinate Gene Silencing in Mature Plants. *Proc. Natl. Acad. Sci. U. S. A.* **2019**, *116*, 7543−7548.
(11) Graham, J. H.; Johnson, E. G.; Myers, M. E.; Young, M.; Rajasekaran, P.; Das, S.; Santra, S. Potential of Nano-Formulated Zinc Oxide for Control of Citrus Canker on Grapefruit Trees. *Plant Dis.* **2016**, *100*, 2442−2447.
(12) Ghosh, D. K.; Kokane, S.; Kumar, P.; Ozcan, A.; Warghane, A.; Motghare, M.; Santra, S.; Sharma, A. K. Antimicrobial Nano-Zinc Oxide-2S Albumin Protein Formulation Significantly Inhibits Growth of "*Candidatus* Liberibacter Asiaticus" in Planta. *PLoS One* **2018**, *13*, No. e0204702.
(13) Lee, W.-M.; An, Y.-J.; Yoon, H.; Kweon, H.-S. Toxicity and Bioavailability of Copper Nanoparticles to the Terrestrial Plants Mung Bean (*Phaseolus Radiatus*) and Wheat (*Triticum Aestivum*): Plant Agar Test for Water-Insoluble Nanoparticles. *Environ. Toxicol. Chem.* **2008**, *27*, 1915.
(14) Cocozza, C.; Perone, A.; Giordano, C.; Salvatici, M. C.; Pignattelli, S.; Raio, A.; Schaub, M.; Sever, K.; Innes, J. L.; Tognetti, R.; Cherubini, P. Silver Nanoparticles Enter the Tree Stem Faster through Leaves than through Roots. *Tree Physiol.* **2019**, *39*, 1251−1261.
(15) Ocsoy, I.; Paret, M. L.; Ocsoy, M. A.; Kunwar, S.; Chen, T.; You, M.; Tan, W. Nanotechnology in Plant Disease Management: DNA-Directed Silver Nanoparticles on Graphene Oxide as an Antibacterial against Xanthomonas Perforans. *ACS Nano* **2013**, *7*, 8972−8980.
(16) Lv, J.; Christie, P.; Zhang, S. Uptake, Translocation, and Transformation of Metal-Based Nanoparticles in Plants: Recent Advances and Methodological Challenges. *Environ. Sci.: Nano* **2019**, *6*, 41−59.
(17) Ma, Y.; He, X.; Zhang, P.; Zhang, Z.; Ding, Y.; Zhang, J.; Wang, G.; Xie, C.; Luo, W.; Zhang, J.; Zheng, L. Xylem and Phloem Based Transport of CeO_2 Nanoparticles in Hydroponic Cucumber Plants. *Environ. Sci. Technol.* **2017**, *51*, 5215−5221.
(18) Hong, J.; Wang, L.; Sun, Y.; Zhao, L.; Niu, G.; Tan, W.; Rico, C. M.; Peralta-Videa, J. R.; Gardea-Torresdey, J. L. Foliar Applied Nanoscale and Microscale CeO_2 and CuO Alter Cucumber (*Cucumis Sativus*) Fruit Quality. *Sci. Total Environ.* **2016**, *563*−*564*, 904−911.
(19) Wang, W.-N.; Tarafdar, J. C.; Biswas, P. Nanoparticle Synthesis and Delivery by an Aerosol Route for Watermelon Plant Foliar Uptake. *J. Nanopart. Res.* **2013**, *15*, 1417.
(20) Wu, H.; Santana, I.; Dansie, J.; Giraldo, J. P. *In Vivo* Delivery of Nanoparticles into Plant Leaves. *Curr. Protoc. Chem. Biol.* **2017**, *9*, 269−284.
(21) Kwak, S. Y.; Giraldo, J. P.; Wong, M. H.; Koman, V. B.; Lew, T. T. S.; Ell, J.; Weidman, M. C.; Sinclair, R. M.; Landry, M. P.; Tisdale, W. A.; Strano, M. S. A Nanobionic Light-Emitting Plant. *Nano Lett.* **2017**, *17*, 7951−7961.
(22) Davis, R. A.; Rippner, D. A.; Hausner, S. H.; Parikh, S. J.; McElrone, A. J.; Sutcliffe, J. L. *In Vivo* Tracking of Copper-64 Radiolabeled Nanoparticles in Lactuca Sativa. *Environ. Sci. Technol.* **2017**, *51*, 12537−12546.
(23) Zhao, L.; Hernandez-Viezcas, J. A.; Peralta-Videa, J. R.; Bandyopadhyay, S.; Peng, B.; Munoz, B.; Keller, A. A.; Gardea-Torresdey, J. L. ZnO Nanoparticle Fate in Soil and Zinc Bioaccumulation in Corn Plants (*Zea Mays*) Influenced by Alginate. *Environ. Sci. Process. Impacts* **2013**, *15*, 260−266.
(24) Graham, J. H.; Johnson, E. G.; Myers, M. E.; Young, M.; Rajasekaran, P.; Das, S.; Santra, S. Potential of Nano-Formulated Zinc Oxide for Control of Citrus Canker on Grapefruit Trees. *Plant Dis.* **2016**, *100*, 2442−2447.
(25) Makhotenko, A. V.; Snigir, E. A.; Kalinina, N. O.; Makarov, V. V.; Taliansky, M. E. Data on a Delivery of Biomolecules into Nicothiana Benthamiana Leaves Using Different Nanoparticles. *Data Br.* **2018**, *16*, 1034−1037.
(26) Hong, J.; Peralta-Videa, J. R.; Rico, C.; Sahi, S.; Viveros, M. N.; Bartonjo, J.; Zhao, L.; Gardea-Torresdey, J. L. Evidence of Translocation and Physiological Impacts of Foliar Applied CeO_2 Nanoparticles on Cucumber (*Cucumis Sativus*) Plants. *Environ. Sci. Technol.* **2014**, *48*, 4376−4385.
(27) Larue, C.; Castillo-Michel, H.; Sobanska, S.; Trcera, N.; Sorieul, S.; Cécillon, L.; Ouerdane, L.; Legros, S.; Sarret, G. Fate of Pristine TiO_2 Nanoparticles and Aged Paint-Containing TiO_2 Nanoparticles in Lettuce Crop after Foliar Exposure. *J. Hazard. Mater.* **2014**, *273*, 17−26.
(28) Su, Y.; Ashworth, V.; Kim, C.; Adeleye, A. S.; Rolshausen, P.; Roper, C.; White, J.; Jassby, D. Delivery, Uptake, Fate, and Transport of Engineered Nanoparticles in Plants: A Critical Review and Data Analysis. *Environ. Sci.: Nano* **2019**, *6*, 2311−2331.
(29) Mondello, V.; Songy, A.; Battiston, E.; Pinto, C.; Coppin, C.; Trotel-Aziz, P.; Clément, C.; Mugnai, L.; Fontaine, F. Grapevine Trunk Diseases: A Review of Fifteen Years of Trials for Their Control with Chemicals and Biocontrol Agents. *Plant Dis.* **2018**, *102*, 1189−1217.
(30) Hu, J.; Jiang, J.; Wang, N. Control of Citrus Huanglongbing *via* Trunk Injection of Plant Defense Activators and Antibiotics. *Phytopathology* **2018**, *108*, 186−195.
(31) Kwak, S.-Y.; Lew, T. T. S.; Sweeney, C. J.; Koman, V. B.; Wong, M. H.; Bohmert-Tatarev, K.; Snell, K. D.; Seo, J. S.; Chua, N.-H.; Strano, M. S. Chloroplast-Selective Gene Delivery and Expression in Planta Using Chitosan-Complexed Single-Walled Carbon Nanotube Carriers. *Nat. Nanotechnol.* **2019**, *14*, 447−455.
(32) Su, Y.; Ashworth, V.; Kim, C.; Adeleye, A. S.; Rolshausen, P.; Roper, C.; White, J.; Jassby, D. Delivery, Uptake, Fate, and Transport of Engineered Nanoparticles in Plants: A Critical Review and Data Analysis. *Environ. Sci.: Nano* **2019**, *6*, 2311−2331.
(33) Jeschke, W. D.; Pate, J. S. Mineral-Nutrition and Transport in Xylem and Phloem of *Banksia Prionotes* (Proteaceae), a Tree with Dimorphic Root Morphology. *J. Exp. Bot.* **1995**, *46*, 895−905.

https://dx.doi.org/10.1021/acsnano.9b07733
ACS Nano 2020, 14, 2966−2981

(34) Shelp, B. J. The Composition of Phloem Exudate and Xylem Sap from Broccoli (*Brassica Oleracea* Var. Italica) Supplied with NH_4^+, NO_3^- or NH_4NO_3. *J. Exp. Bot.* **1987**, *38*, 1619−1636.
(35) Santiago, M.; Pagay, V.; Stroock, A. D. Impact of Electroviscosity on the Hydraulic Conductance of the Bordered Pit Membrane: A Theoretical Investigation. *Plant Physiol.* **2013**, *163*, 999−1011.
(36) Jansen, S.; Choat, B.; Pletsers, A. Morphological Variation of Intervessel Pit Membranes and Implications to Xylem Function in Angiosperms. *Am. J. Bot.* **2009**, *96*, 409−419.
(37) Hijaz, F.; Killiny, N. Collection and Chemical Composition of Phloem Sap from *Citrus Sinensis* L. Osbeck (Sweet Orange). *PLoS One* **2014**, *9*, e101830.
(38) Choat, B.; Munns, R.; McCully, M.; Passioura, J.; Tyerman, S.; Canny, M.; Bramley, H.; Al, E. Chapter 3—Water Movement in Plants. In *Plants In Action*; Choat, B., Munns, R., Eds.; Australian Society of Plant Scientists; Macmillan Education Australia Pty Ltd: Melbourne, Australia, 2010; pp 1−63; http://plantsinaction.science.uq.edu.au/content/Chapter-3-water-movement-plants (accessed 2/14/2018).
(39) McCulloh, K. A.; Sperry, J. S.; Adler, F. R. Water Transport in Plants Obeys Murray's Law. *Nature* **2003**, *421*, 939−942.
(40) Brant, J.; Lecoanet, H.; Wiesner, M. R. Aggregation and Deposition Characteristics of Fullerene Nanoparticles in Aqueous Systems. *J. Nanopart. Res.* **2005**, *7*, 545−553.
(41) Schwabe, F.; Schulin, R.; Limbach, L. K.; Stark, W.; Bürge, D.; Nowack, B. Influence of Two Types of Organic Matter on Interaction of CeO_2 Nanoparticles with Plants in Hydroponic Culture. *Chemosphere* **2013**, *91*, 512−520.
(42) Adeleye, A. S.; Keller, A. A. Interactions between Algal Extracellular Polymeric Substances and Commercial TiO_2 Nanoparticles in Aqueous Media. *Environ. Sci. Technol.* **2016**, *50*, 12258−12265.
(43) Levard, C.; Mitra, S.; Yang, T.; Jew, A. D.; Badireddy, A. R.; Lowry, G. V.; Brown, G. E. Effect of Chloride on the Dissolution Rate of Silver Nanoparticles and Toxicity to E. Coli. *Environ. Sci. Technol.* **2013**, *47*, 5738−5745.
(44) Dahle, J. T.; Livi, K.; Arai, Y. Effects of pH and Phosphate on CeO_2 Nanoparticle Dissolution. *Chemosphere* **2015**, *119*, 1365−1371.
(45) Li, Y.; Chen, H.; Wang, F.; Zhao, F.; Han, X.; Geng, H.; Gao, L.; Chen, H.; Yuan, R.; Yao, J. Environmental Behavior and Associated Plant Accumulation of Silver Nanoparticles in the Presence of Dissolved Humic and Fulvic Acid. *Environ. Pollut.* **2018**, *243*, 1334−1342.
(46) Adeleye, A. S.; Conway, J. R.; Perez, T.; Rutten, P.; Keller, A. A. Influence of Extracellular Polymeric Substances on the Long-Term Fate, Dissolution, and Speciation of Copper-Based Nanoparticles. *Environ. Sci. Technol.* **2014**, *48*, 12561−12568.
(47) Adeleye, A. S.; Stevenson, L. M.; Su, Y.; Nisbet, R. M.; Zhang, Y.; Keller, A. A. Influence of Phytoplankton on Fate and Effects of Modified Zerovalent Iron Nanoparticles. *Environ. Sci. Technol.* **2016**, *50*, 5597−5605.
(48) Wiesner, M. R.; Bottero, J. *Environmental Nanotechnology: Applications and Impacts of Nanomaterials*; 2nd ed.; McGraw-Hill Education: New York, 2017.
(49) Avellan, A.; Yun, J.; Zhang, Y.; Spielman-Sun, E.; Unrine, J. M.; Thieme, J.; Li, J.; Lombi, E.; Bland, G.; Lowry, G. V. Nanoparticle Size and Coating Chemistry Control Foliar Uptake Pathways, Translocation, and Leaf-to-Rhizosphere Transport in Wheat. *ACS Nano* **2019**, *13*, 5291−5305.
(50) Dan, Y.; Zhang, W.; Xue, R.; Ma, X.; Stephan, C.; Shi, H. Characterization of Gold Nanoparticle Uptake by Tomato Plants Using Enzymatic Extraction Followed by Single-Particle Inductively Coupled Plasma-Mass Spectrometry Analysis. *Environ. Sci. Technol.* **2015**, *49*, 3007−3014.
(51) Schwab, F.; Zhai, G.; Kern, M.; Turner, A.; Schnoor, J. L.; Wiesner, M. R. Barriers, Pathways and Processes for Uptake, Translocation and Accumulation of Nanomaterials in Plants − Critical Review. *Nanotoxicology* **2016**, *5390*, 1−22.
(52) Wang, P.; Lombi, E.; Zhao, F. J.; Kopittke, P. M. Nanotechnology: A New Opportunity in Plant Sciences. *Trends Plant Sci.* **2016**, *21*, 699−712.
(53) Larue, C.; Laurette, J.; Herlin-Boime, N.; Khodja, H.; Fayard, B.; Flank, A. M.; Brisset, F.; Carriere, M. Accumulation, Translocation and Impact of TiO_2 Nanoparticles in Wheat (*Triticum Aestivum* spp.): Influence of Diameter and Crystal Phase. *Sci. Total Environ.* **2012**, *431*, 197−208.
(54) Etxeberria, E.; Gonzalez, P.; Bhattacharya, P.; Sharma, P.; Ke, P. C. Determining the Size Exclusion for Nanoparticles in Citrus Leaves. *HortScience* **2016**, *51*, 732−737.
(55) Majumdar, S.; Ma, C.; Villani, M.; Zuverza-Mena, N.; Pagano, L.; Huang, Y.; Zappettini, A.; Keller, A. A.; Marmiroli, N.; Dhankher, O. P.; White, J. C. Surface Coating Determines the Response of Soybean Plants to Cadmium Sulfide Quantum Dots. *NanoImpact* **2019**, *14*, 100151.
(56) Majumdar, S.; Pagano, L.; Wohlschlegel, J. A.; Villani, M.; Zappettini, A.; White, J. C.; Keller, A. A. Proteomic, Gene and Metabolite Characterization Reveal the Uptake and Toxicity Mechanisms of Cadmium Sulfide Quantum Dots in Soybean Plants. *Environ. Sci.: Nano* **2019**, *6*, 3010−3026.
(57) Delay, M.; Dolt, T.; Woellhaf, A.; Sembritzki, R.; Frimmel, F. H. Interactions and Stability of Silver Nanoparticles in the Aqueous Phase: Influence of Natural Organic Matter (NOM) and Ionic Strength. *J. Chromatogr. A* **2011**, *1218*, 4206−4212.
(58) Trujillo-Reyes, J.; Vilchis-Nestor, A. R.; Majumdar, S.; Peralta-Videa, J. R.; Gardea-Torresdey, J. L. Citric Acid Modifies Surface Properties of Commercial CeO_2 Nanoparticles Reducing Their Toxicity and Cerium Uptake in Radish (*Raphanus Sativus*) Seedlings. *J. Hazard. Mater.* **2013**, *263*, 677−684.
(59) Lead, J. R.; Batley, G. E.; Alvarez, P. J. J.; Croteau, M.-N.; Handy, R. D.; McLaughlin, M. J.; Judy, J. D.; Schirmer, K. Nanomaterials in the Environment: Behavior, Fate, Bioavailability, and Effects-An Updated Review. *Environ. Toxicol. Chem.* **2018**, *37*, 2029−2063.
(60) Zhu, Z.-J.; Wang, H.; Yan, B.; Zheng, H.; Jiang, Y.; Miranda, O. R.; Rotello, V. M.; Xing, B.; Vachet, R. W. Effect of Surface Charge on the Uptake and Distribution of Gold Nanoparticles in Four Plant Species. *Environ. Sci. Technol.* **2012**, *46*, 12391−12398.
(61) Koo, Y.; Wang, J.; Zhang, Q.; Zhu, H.; Chehab, E. W.; Colvin, V. L.; Alvarez, P. J. J.; Braam, J. Fluorescence Reports Intact Quantum Dot Uptake into Roots and Translocation to Leaves of *Arabidopsis Thaliana* and Subsequent Ingestion by Insect Herbivores. *Environ. Sci. Technol.* **2015**, *49*, 626−632.
(62) Song, J. E.; Phenrat, T.; Marinakos, S.; Xiao, Y.; Liu, J.; Wiesner, M. R.; Tilton, R. D.; Lowry, G. V. Hydrophobic Interactions Increase Attachment of Gum Arabic- and PVP-Coated Ag Nanoparticles to Hydrophobic Surfaces. *Environ. Sci. Technol.* **2011**, *45*, 5988−5995.
(63) Vasicek, T. W.; Jenkins, S. V.; Vaz, L.; Chen, J.; Stenken, J. A. Thermoresponsive Nanoparticle Agglomeration/Aggregation in Salt Solutions: Dependence on Graft Density. *J. Colloid Interface Sci.* **2017**, *506*, 338−345.
(64) Eaton, F. M. Toxicity and Accumulation of Chloride and Sulfate Salts in Plants. *J. Agric. Res.* **1942**, *64*, 357−399.
(65) Moya, J. L.; Primo-Millo, E.; Talon, M. Morphological Factors Determining Salt Tolerance in Citrus Seedlings: The Shoot to Root Ratio Modulates Passive Root Uptake of Chloride Ions and Their Accumulation in Leaves. *Plant, Cell Environ.* **1999**, *22*, 1425−1433.
(66) Mason, T. G.; Phillis, E. Studies on the Partition of the Mineral Elements in the Cotton Plant. *Ann. Bot.* **1945**, *9*, 335−344.
(67) Peuke, A. D.; Gessler, A.; Tcherkez, G. Experimental Evidence for Diel δ^{15}N-patterns in Different Tissues, Xylem and Phloem Saps of Castor Bean (*Ricinus Communis* L.). *Plant, Cell Environ.* **2013**, *36*, 2219−2228.
(68) Comunian, T. A.; Favaro-Trindade, C. S. Microencapsulation Using Biopolymers as an Alternative to Produce Food Enhanced with Phytosterols and Omega-3 Fatty Acids: A Review. *Food Hydrocolloids* **2016**, *61*, 442−457.

https://dx.doi.org/10.1021/acsnano.9b07733
ACS Nano 2020, 14, 2966−2981

(69) Chanamai, R.; McClements, D. J. Comparison of Gum Arabic, Modified Starch, and Whey Protein Isolate as Emulsifiers: Influence of pH, $CaCl_2$ and Temperature. *J. Food Sci.* **2002**, *67*, 120−125.
(70) Koczkur, K. M.; Mourdikoudis, S.; Polavarapu, L.; Skrabalak, S. E. Polyvinylpyrrolidone (PVP) in Nanoparticle Synthesis. *Dalt. Trans.* **2015**, *44*, 17883−17905.
(71) Baker, J. A.; Pearson, R. A.; Berg, J. C. Influence of Particle Curvature on Polymer Adsorption Layer Thickness. *Langmuir* **1989**, *5*, 339−342.
(72) Ohshima, H. Electrophoresis of Soft Particles. *Adv. Colloid Interface Sci.* **1995**, *62*, 189−235.
(73) Zhang, Y.; Klepsch, M.; Jansen, S. Bordered Pits in Xylem of Vesselless Angiosperms and Their Possible Misinterpretation as Perforation Plates. *Plant, Cell Environ.* **2017**, *40*, 2133−2146.
(74) Jensen, K. H.; Mullendore, D. L.; Holbrook, N. M.; Bohr, T.; Knoblauch, M.; Bruus, H. Modeling the Hydrodynamics of Phloem Sieve Plates. *Front. Plant Sci.* **2012**, *3*, 1−11.
(75) Choat, B.; Ball, M.; Luly, J.; Holtum, J. Pit Membrane Porosity and Water Stress-Induced Cavitation in Four Co-Existing Dry Rainforest Tree Species. *Plant Physiol.* **2003**, *131*, 41−48.
(76) Choat, B.; Brodie, T. W.; Cobb, A. R.; Zwieniecki, M. A.; Holbrook, N. M. Direct Measurements of Intervessel Pit Membrane Hydraulic Resistance in Two Angiosperm Tree Species. *Am. J. Bot.* **2006**, *93*, 993−1000.
(77) McElrone, A. J.; Jackson, S.; Habdas, P. Hydraulic Disruption and Passive Migration by a Bacterial Pathogen in Oak Tree Xylem. *J. Exp. Bot.* **2008**, *59*, 2649−2657.
(78) Carlquist, S.; Schneider, E. L. Vessels of *Illicium* (Illiciaceae): Range of Pit Membrane Remnant Presence in Perforations and Other Vessel Details. *Int. J. Plant Sci.* **2002**, *163*, 755−763.
(79) Houterman, P. M.; Speijer, D.; Dekker, H. L.; DE Koster, C. G.; Cornelissen, B. J. C.; Rep, M. The Mixed Xylem Sap Proteome of Fusarium Oxysporum-Infected Tomato Plants. *Mol. Plant Pathol.* **2007**, *8*, 215−221.
(80) Kehr, J. Phloem Sap Proteins: Their Identities and Potential Roles in the Interaction between Plants and Phloem-Feeding Insects. *J. Exp. Bot.* **2006**, *57*, 767−774.
(81) Spielman-Sun, E.; Avellan, A.; Bland, G. D.; Clement, E. T.; Tappero, R.; Acerbo, A.; Lowry, G. V. Protein Coating Composition Targets Nanoparticles to Leaf Stomata and Trichomes. *Nanoscale* **2020**, *12*, 3630−3636.
(82) Ma, R.; Levard, C.; Marinakos, S. M.; Cheng, Y.; Liu, J.; Michel, F. M.; Brown, G. E.; Lowry, G. V. Size-Controlled Dissolution of Organic-Coated Silver Nanoparticles. *Environ. Sci. Technol.* **2012**, *46*, 752−759.
(83) Li, X.; Lenhart, J. J.; Walker, H. W. Aggregation Kinetics and Dissolution of Coated Silver Nanoparticles. *Langmuir* **2012**, *28*, 1095−1104.
(84) Li, X.; Lenhart, J. J. Aggregation and Dissolution of Silver Nanoparticles in Natural Surface Water. *Environ. Sci. Technol.* **2012**, *46*, 5378−5386.
(85) Liu, J.; Hurt, R. H. Ion Release Kinetics and Particle Persistence in Aqueous Nano-Silver Colloids. *Environ. Sci. Technol.* **2010**, *44*, 2169−2175.
(86) Zhang, W.; Yao, Y.; Sullivan, N.; Chen, Y. Modeling the Primary Size Effects of Citrate-Coated Silver Nanoparticles on Their Ion Release Kinetics. *Environ. Sci. Technol.* **2011**, *45*, 4422−4428.
(87) Peretyazhko, T. S.; Zhang, Q.; Colvin, V. L. Size-Controlled Dissolution of Silver Nanoparticles at Neutral and Acidic PH Conditions: Kinetics and Size Changes. *Environ. Sci. Technol.* **2014**, *48*, 11954−11961.
(88) Zhang, W.; Qiao, X.; Chen, J.; Wang, H. Preparation of Silver Nanoparticles in Water-in-Oil AOT Reverse Micelles. *J. Colloid Interface Sci.* **2006**, *302*, 370−373.
(89) Venkata, K. R. P.; Venkata, A. K.; Karthik, P. S.; Surya, P. S. Conductive Silver Inks and Their Applications in Printed and Flexible Electronics. *RSC Adv.* **2015**, *5*, 77760−77790.
(90) Han, L.; Wang, P.; Zhu, C.; Zhai, Y.; Dong, S. Facile Solvothermal Synthesis of Cube-like Ag@AgCl: A Highly Efficient Visible Light Photocatalyst. *Nanoscale* **2011**, *3*, 2931.
(91) Chen, S.-F.; Zhang, H.; Lin, Q.-Y. Effect of Different Water Conditions on Dissolution of Nanosilver. *Water Sci. Technol.* **2013**, *68*, 1745−1750.
(92) Zhang, P.; Ma, Y.; Liu, S.; Wang, G.; Zhang, J.; He, X.; Zhang, J.; Rui, Y.; Zhang, Z. Phytotoxicity, Uptake and Transformation of Nano-CeO_2 in Sand Cultured Romaine Lettuce. *Environ. Pollut.* **2017**, *220*, 1400−1408.
(93) Morones, J. R.; Elechiguerra, J. L.; Camacho, A.; Holt, K.; Kouri, J. B.; Ramírez, J. T.; Yacaman, M. J. The Bactericidal Effect of Silver Nanoparticles. *Nanotechnology* **2005**, *16*, 2346−2353.
(94) Milewska-Hendel, A.; Zubko, M.; Karcz, J.; Stróż, D.; Kurczyńska, E. Fate of Neutral-Charged Gold Nanoparticles in the Roots of the Hordeum Vulgare L. Cultivar Karat. *Sci. Rep.* **2017**, *7*, 1−13.
(95) Whiteside, M. D.; Treseder, K. K.; Atsatt, P. R. The Brighter Side of Soils: Quantum Dots Track Organic Nitrogen through Fungi and Plants. *Ecology* **2009**, *90*, 100−108.
(96) Du, W.; Sun, Y.; Ji, R.; Zhu, J.; Wu, J.; Guo, H. TiO_2 and ZnO Nanoparticles Negatively Affect Wheat Growth and Soil Enzyme Activities in Agricultural Soil. *J. Environ. Monit.* **2011**, *13*, 822.
(97) Al-Salim, N.; Barraclough, E.; Burgess, E.; Clothier, B.; Deurer, M.; Green, S.; Malone, L.; Weir, G. Quantum Dot Transport in Soil, Plants, and Insects. *Sci. Total Environ.* **2011**, *409*, 3237−3248.
(98) Avellan, A.; Yun, J.; Zhang, Y.; Spielman-Sun, E.; Unrine, J. M.; Thieme, J.; Li, J.; Lombi, E.; Bland, G.; Lowry, G. V. Nanoparticle Size and Coating Chemistry Control Foliar Uptake Pathways, Translocation, and Leaf-to-Rhizosphere Transport in Wheat. *ACS Nano* **2019**, *13*, 5291−5305.
(99) Podila, R.; Chen, R.; Ke, P. C.; Brown, J. M.; Rao, A. M. Effects of Surface Functional Groups on the Formation of Nanoparticle-Protein Corona. *Appl. Phys. Lett.* **2012**, *101*, 263701.
(100) Hawthorne, J.; Musante, C.; Sinha, S. K.; White, J. C. Accumulation and Phytotoxicity of Engineered Nanoparticles to Cucurbita Pepo. *Int. J. Phytorem.* **2012**, *14*, 429−442.
(101) Zhao, L.; Sun, Y.; Hernandez-Viezcas, J. A.; Hong, J.; Majumdar, S.; Niu, G.; Duarte-Gardea, M.; Peralta-Videa, J. R.; Gardea-Torresdey, J. L. Monitoring the Environmental Effects of CeO_2 and ZnO Nanoparticles through the Life Cycle of Corn (Zea Mays) Plants and *In Situ* μ-XRF Mapping of Nutrients in Kernels. *Environ. Sci. Technol.* **2015**, *49*, 2921−2928.
(102) Zhai, G.; Walters, K. S.; Peate, D. W.; Alvarez, P. J. J.; Schnoor, J. L. Transport of Gold Nanoparticles through Plasmodesmata and Precipitation of Gold Ions in Woody Poplar. *Environ. Sci. Technol. Lett.* **2014**, *1*, 146−151.
(103) Ma, C.; Chhikara, S.; Minocha, R.; Long, S.; Musante, C.; White, J. C.; Xing, B.; Dhankher, O. P. Reduced Silver Nanoparticle Phytotoxicity in Crambe Abyssinica with Enhanced Glutathione Production by Overexpressing Bacterial γ-Glutamylcysteine Synthase. *Environ. Sci. Technol.* **2015**, *49*, 10117−10126.
(104) Wang, J.; Koo, Y.; Alexander, A.; Yang, Y.; Westerhof, S.; Zhang, Q.; Schnoor, J. L.; Colvin, V. L.; Braam, J.; Alvarez, P. J. J. Phytostimulation of Poplars and Arabidopsis Exposed to Silver Nanoparticles and Ag+ at Sublethal Concentrations. *Environ. Sci. Technol.* **2013**, *47*, 5442−5449.
(105) Strozyk, M. S.; Chanana, M.; Pastoriza-Santos, I.; Pérez-Juste, J.; Liz-Marzán, L. M. Protein/Polymer-Based Dual-Responsive Gold Nanoparticles with PH-Dependent Thermal Sensitivity. *Adv. Funct. Mater.* **2012**, *22*, 1436−1444.
(106) Rovira, A. D. Plant Root Exudates. *Bot. Rev.* **1969**, *35*, 35−57.
(107) Borisjuk, N. V.; Borisjuk, L. G.; Logendra, S.; Petersen, F.; Gleba, Y.; Raskin, I. Production of Recombinant Proteins in Plant Root Exudates. *Nat. Biotechnol.* **1999**, *17*, 466−469.
(108) Rohrbacher, F.; St-Arnaud, M. Root Exudation: The Ecological Driver of Hydrocarbon Rhizoremediation. *Agronomy* **2016**, *6*, 19.

https://dx.doi.org/10.1021/acsnano.9b07733
ACS Nano 2020, 14, 2966−2981

(109) Johnson, E. G.; Wu, J.; Bright, D. B.; Graham, J. H. Association of 'Candidatus Liberibacter Asiaticus' Root Infection, but Not Phloem Plugging with Root Loss on Huanglongbing-Affected Trees Prior to Appearance of Foliar Symptoms. *Plant Pathol.* **2014**, *63*, 290−298.
(110) Ge, L.; Han, C.; Liu, J.; Li, Y. Enhanced Visible Light Photocatalytic Activity of Novel Polymeric G-C3N4 Loaded with Ag Nanoparticles. *Appl. Catal., A* **2011**, *409*−*410*, 215−222.
(111) Nikinmaa, E.; Hölttä, T.; Hari, P.; Kolari, P.; Mäkelä, A.; Sevanto, S.; Vesala, T. Assimilate Transport in Phloem Sets Conditions for Leaf Gas Exchange. *Plant, Cell Environ.* **2013**, *36*, 655−669.
(112) Hölttä, T.; Nikinmaa, E. Modelling the Effect of Xylem and Phloem Transport on Leaf Gas Exchange. *Acta Hortic.* **2013**, *991*, 351−358.
(113) Yang, X.; Gondikas, A. P.; Marinakos, S. M.; Auffan, M.; Liu, J.; Hsu-Kim, H.; Meyer, J. N. Mechanism of Silver Nanoparticle Toxicity Is Dependent on Dissolved Silver and Surface Coating in Caenorhabditis Elegans. *Environ. Sci. Technol.* **2012**, *46*, 1119−1127.
(114) Gessler, A.; Rennenberg, H.; Keitel, C. Stable Isotope Composition of Organic Compounds Transported in the Phloem of European Beech - Evaluation of Different Methods of Phloem Sap Collection and Assessment of Gradients in Carbon Isotope Composition during Leaf-to-Stem Transport. *Plant Biol.* **2004**, *6*, 721−729.
(115) Lin, D.; Xing, B. Root Uptake and Phytotoxicity of ZnO Nanoparticles. *Environ. Sci. Technol.* **2008**, *42*, 5580−5585.

https://dx.doi.org/10.1021/acsnano.9b07733
ACS Nano 2020, 14, 2966−2981